Stromal SPARC contributes to the detrimental fibrotic changes associated with myeloproliferation whereas its deficiency favors myeloid cell expansion

*Claudio Tripodo,[1] *Sabina Sangaletti,[2] Carla Guarnotta,[1] Pier P. Piccaluga,[3] Matilde Cacciatore,[1] Michela Giuliano,[4] Giovanni Franco,[5] Claudia Chiodoni,[2] Marika Sciandra,[6] Silvia Miotti,[2] Giuseppe Calvaruso,[4] Alessandra Carè,[7] Ada M. Florena,[1] Katia Scotlandi,[6] Attilio Orazi,[8] Stefano A. Pileri,[3] and Mario P. Colombo[2]

[1]Tumor Immunology Unit, Human Pathology Section, Department of Health Sciences, University of Palermo, Palermo, Italy; [2]Molecular Immunology Unit, Department of Experimental Oncology and Molecular Medicine, Fondazione Istituto di Ricovero e Cura a Carattere Scientifico Istituto Nazionale Tumori, Milan, Italy; [3]Department of Hematology and Oncological Sciences L.e.A. Seràgnoli, University of Bologna School of Medicine, Bologna, Italy; [4]Section of Biochemical Sciences, Department of Experimental Medicine and Neuroscience, University of Palermo, Palermo, Italy; [5]Hematology Unit, Department of Oncology and Hematology, University of Palermo, Palermo, Italy; [6]Laboratory of Experimental Oncology, CRS Development of Biomolecular Therapies, Istituto di Ricovero e Cura a Carattere Scientifico Rizzoli Institute, Bologna, Italy; [7]Department of Hematology, Oncology and Molecular Medicine, Istituto Superiore di Sanità, Rome, Italy; and [8]Hematopathology Division, Department of Pathology and Laboratory Medicine, Weill Cornell Medical College, New York, NY

In myeloid malignancies, the neoplastic clone outgrows normal hematopoietic cells toward BM failure. This event is also sustained by detrimental stromal changes, such as BM fibrosis and osteosclerosis, whose occurrence is harbinger of a dismal prognosis. We show that the matricellular protein SPARC contributes to the BM stromal response to myeloproliferation. The degree of SPARC expression in BM stromal elements, including CD146$^+$ mesenchymal stromal cells, correlates with the degree of stromal changes, and the severity of BM failure characterizing the prototypical myeloproliferative neoplasm primary myelofibrosis. Using *Sparc*$^{-/-}$ mice and BM chimeras, we demonstrate that SPARC contributes to the development of significant stromal fibrosis in a model of thrombopoietin-induced myelofibrosis. We found that SPARC deficiency in the radioresistant BM stroma compartment impairs myelofibrosis but, at the same time, associates with an enhanced reactive myeloproliferative response to thrombopoietin. The link betwen SPARC stromal deficiency and enhanced myeloid cell expansion under a myeloproliferative spur is also supported by the myeloproliferative phenotype resulting from the transplantation of defective *Apc*^{min} mutant hematopoietic cells into *Sparc*$^{-/-}$ but not WT recipient BM stroma. Our results highlight a complex influence of SPARC over the stromal and hematopoietic BM response in myeloproliferative conditions. (*Blood*. 2012;120(17):3541-3554)

Introduction

Bone marrow (BM) homeostasis stems from the regulated crosstalk between hematopoietic and stromal components. Through this interaction, hematopoietic stem cells (HSCs) are kept in a quiescent state or driven toward differentiation. This crosstalk occurs within specific stromal microenvironments termed "niches."[1] The osteoblastic/endosteal niche is composed of endosteal fibroblasts, osteoblasts, and bone-related extracellular matrix (ECM), the vascular niche of endothelial cells and adventitial reticular cells. Signals originating in these microenvironments orchestrate hematopoietic cell localization, maturation, and mobilization dynamics responsible for normal hematopoiesis,[1] whereas a biased stromal niche can lead to altered hematopoiesis, toward leukemogenesis.[2]

In myeloid malignancies, neoplastic clone expansion alters the composition of the BM parenchyma and results in impaired hematopoiesis and BM failure.[3-5] In addition to direct replacement of normal hematopoiesis, neoplastic proliferation generates detrimental alterations in the BM stroma.[6-9] BM stromal changes associated with myeloproliferation include excessive ECM deposition, which manifest as BM fibrosis,[6-7] neoangiogenesis,[8] and bone abnormalities (osteosclerosis).[6-7,9] These changes are variably observed in acute myeloid leukemias (AMLs), myelodysplastic syndromes (MDSs), and myeloproliferative neoplasms.[6] In neoplasms characterized by a more gradual myeloproliferation, the development of BM stroma alterations can represent the only sign of disease progression.[5,10]

BM stromal alterations are of prognostic significance in myeloid malignancies. BM fibrosis is associated with a more aggressive disease course and worse prognosis in patients with both myeloproliferative neoplasm and MDS.[6,11-15] In myeloproliferative neoplasm, stromal changes may eventually cause the disruption of normal HSC niches, which inhibits the growth of resident hematopoietic elements and results in the establishment of extramedullary hematopoiesis.[3-6,16] Moreover, stromal alterations may render the HSC niche unfit for HSC seeding (supplemental Figure 1) and negatively impact the outcome of allogeneic stem cell transplantation.[17,18] Thus, BM stroma involvement in myeloid malignancies is an integral part of the disease manifestations impacting the outcome. However, little is known about the nature of stroma-intrinsic factors and their role in BM stromal changes and myeloid clone progression.

Secreted protein acidic and rich in cysteine (SPARC), also known as osteonectin or BM-40, is a matricellular protein that

Submitted December 14, 2011; accepted August 18, 2012. Prepublished online as *Blood* First Edition paper, September 5, 2012; DOI 10.1182/blood-2011-12-398537.

*C.T. and S.S. contributed equally to this study.

The publication costs of this article were defrayed in part by page charge payment. Therefore, and solely to indicate this fact, this article is hereby marked "advertisement" in accordance with 18 USC section 1734.

Table 1. Presenting clinical and laboratory features of myeloid neoplasm and control cases

	AML	MDS	ET	PV	PMF	Control
No. of cases	10	10	12	10	24	16
Mean age, y (range)	56.1 (31-77)	60.8 (36-80)	64.3 (30-80)	58.5 (34-85)	65.5 (40-86)	52.5 (21-85)
Sex, %						
Male	27.2	50	83.3	30	58.3	43.7
Female	72.8	50	16.67	70	41.7	56.3
Cellularity, %*	80 (10-100)	68 (60-90)	43 (35-60)	83 (40-100)	75 (50-100)	48 (25-85)
Fibrosis grade†	1	2	1	1	1	0
Grade 0	0	0	33.3	0	8.4	50
Grade 1	70	40	66.6	60	45.8	50
Grade 2	20	50	0	20	20.8	0
Grade 3	10	10	0	20	25	0
WBC count, $\times 10^9$/L*	63.8 (1.6-420)	3.2 (1.2-5.2)	8.2 (4.1-13.2)	11.4 (4.9-22.6)	12 (2.3-51.5)	9.1 (2.2-14.6)
Hb, g/L*	83.6 (64-95)	88 (62-142)	130.6 (102-146)	160 (100-210)	122 (81-150)	128 (88-159)
PLT count, $\times 10^9$/L*	52.1 (16-146)	107.8 (19-264)	737.8 (411-942)	292.9 (126-494)	463.5 (13-1218)	305.9 (143-762)

*Values are mean (range).
†Fibrosis grade is reported as median (%) of each grade. Fibrosis is evaluated according to Thiele et al.[7]

plays a major role in the maintenance and restoration of tissue homeostasis.[19] SPARC has been implicated in tissue remodeling during embryogenesis, wound healing, immune responses,[20] cancer stromatogenesis, and epithelial-to-mesenchymal transition.[19-21]

In myeloid malignancies, *SPARC* (5q31.3–32) deletion has been associated with 5q− MDS,[22] and low or absent SPARC expression has been reported in a subset of AML.[23] Conversely, SPARC overexpression characterizes CML cells displaying resistance to imatinib in vitro, suggesting a role in myeloid clone progression.[24]

Herein, we investigated the role of SPARC in the BM stromal alterations associated with myeloproliferation. Altogether, our results suggest that stromal SPARC plays a key role in sustaining the detrimental fibrosis that occurs in myeloid malignancies and reveal SPARC's influence on the BM hematopoietic response in myeloproliferative conditions.

Methods

Patient samples

BM trephine biopsies (BMBs) of patients with myeloid malignancies were selected from the archives of the Human Pathology Section, University of Palermo. Ten consecutive AML cases, 10 MDS, 12 essential thrombocytemia, 10 polycythemia vera (PV), and 56 primary myelofibrosis (PMF) cases diagnosed between December 2008 and January 2011, according to the 2008 WHO classification criteria,[3] were included. Ten BMBs from patients with reactive thrombocytosis and 6 BMBs of patients with Hodgkin lymphoma without marrow involvement were used as controls. Only representative BMBs[8] collected at the time of diagnosis were included. For all of the cases, the following presenting data were retrieved from the patients' medical records: age, sex, hemoglobin levels (Hb), peripheral blood (PB) leukocyte count (white blood cell count), and platelet count (PLT; Tables 1 and 2). All of the procedures were in accordance with the Declaration of Helsinki.

Mice

BALB/cAnNCrl mice, 8-10 weeks old, were purchased from Charles River Laboratories. The CNCr.129S(B6)–Sparctm1Hwe mice were developed in our animal facility as previously described.[25] *Apc^{min}* mice (B6, Ly5b) were a kind gift of Dr Antonio Sica (Fondazione Istituto Clinico Humanitas). Chimeric *Sparc*$^{-/-}$ > wild-type (WT; Thy-1b > Thy-1a), WT > *Sparc*$^{-/-}$(Thy-1a > Thy-1b), WT > WT(Thy-1a > Thy-1b), *Sparc*$^{-/-}$ > *Sparc*$^{-/-}$(Thy-1b > Thy-1b), *Apc^{min}* > WT (Ly5b > Ly5a), and *Apc^{min}* > *Sparc*$^{-/-}$ (Ly5b > Ly5a) mice were obtained by BM transplantation as previously reported.[25] Engraftment was verified 6-8 weeks after BM transplantation by FACS analysis of PB mononuclear cells according to Thy-1a (BD Biosciences) and Thy-1b (BD Biosciences) or Ly5a (BD Biosciences), and Ly5b (BD Biosciences) expression. The animal experiments were authorized by the Institutional Ethical Committee for Animal Use.

Table 2. Presenting clinical and laboratory data of the 56 PMF cases

	Prefibrotic/early fibrotic (grade 0/1)*	Advanced fibrotic (grade 2/3)*	*P*†	Low/intermediate-1 risk‡	Intermediate-2/ high risk‡	*P*†
Sex, no. (%)						
Male	9 (29)	14 (56)		14 (30.4)	9 (90)	
Female	22 (71)	11 (44)		32 (69.6)	1 (10)	
Age (y) at diagnosis*	63 (25-86)	65 (44-86)	.86	62 (25-88)	71 (57-79)	.1
Hb, g/L	131.6 (92-172)	111 (80-164)	.0003	127.7 (87-172)	98 (80-127)	.0004
WBC, $\times 10^9$/L	9.6 (3.8-15)	11.9 (2.8-51.5)	.67	10.3 (3.8-22.1)	12.1 (2.8-51.5)	.2
PLT, $\times 10^9$/L	662.7 (200-1218)	401 (49-1031)	.004	605 (121-1218)	304 (490-753)	.01
Cellularity, %	60.8 (20-90)	71.6 (30-100)	.02	62.9 (20-100)	78 (50-90)	.008
SPARC$^+$ stromal cells × HPF	3.9 (0.5-15.9)	6.7 (2.4-15.7)	.0003	4.7 (0.5-15.9)	7.3 (1.4-15.7)	.004
CD146$^+$ stromal cells × HPF	6 (1-12.2)	10.2 (3.8-23.5)	.0004	7.5 (1-23.5)	9.3 (3-21)	.4
MVD × HPF	5.8 (1-12.2)	9.9 (2.8-18.6)	.00001	6.5 (1.6-18.6)	8.5 (3-14.8)	.1

Values are mean (range). HPF (×400).
*Fibrosis was evaluated according to Thiele et al.[7]
†According to Mann-Whitney *U* test.
‡According to Cervantes et al.[31]

In vivo recombinant TPO treatment

Recombinant murine thrombopoietin (TPO; PeproTech) or sterile saline was injected intraperitoneally into WT, Sparc$^{-/-}$, and chimeric mice once daily (500 μg/kg) for 10 or 14 consecutive days.[26] After treatment, PB was collected and analyzed for Hb, PLT, and circulating Gr1$^+$CD11b$^+$ myeloid cells. At the same time point, the mice were killed and their spleen, femurs, and tibias were collected for histopathologic/immunophenotypical and FACS analyses and for BM colony formation assays.

Histopathology and immunohistochemistry

Histopathologic analysis was performed on formalin-fixed, paraffin-embedded specimens as previously reported.[9,25] Four-micrometer-thick sections were routinely stained with hematoxylin and eosin, Gomori reticulin, and Masson trichrome stain.

The degree of BM fibrosis on human BMBs was semiquantitatively assessed on Gomori-stained sections according to the European Consensus Grading System,[7] which ranges from 0 (normal BM fiber content) to 3 (diffuse and dense increase in reticulin with extensive intersections of coarse collagen bundles, associated with osteosclerosis). A similar semiquantitative system was also adopted for BM fibrosis evaluation on Gomori-stained mouse BM sections.

Immunohistochemistry was performed using the streptavidin-biotin-peroxidase complex method as previously reported.[9] The antibodies adopted for immunohistochemistry are listed in supplemental Methods.

The slides were analyzed under a Leica-DM2000 optical microscope (Leica Microsystems) using Leica 10× SL, HI PLAN 20×/0.40, HI PLAN 40×/0.65, HI PLAN 63×/0.75, and PL FLUOTAR 100×/1.30 objectives, and microphotographs were collected using a Leica-DFC320 digital camera and the Leica-IM50 Version 4.0 acquisition software (Leica Microsystems).

The number of SPARC$^+$ and CD146$^+$ stromal cells was determined on immunostained sections by counting the absolute number of reactive cells with stromal morphology within 10 different high-power fields (HPFs; ×400 magnification) and then averaging the counts obtained from the 10 fields. Similarly, microvascular density (MVD) was determined by counting the number of CD34$^+$ vascular structures, as previously reported.[9] Differential hematopoietic cell counts on mouse BM sections were performed by counting the absolute number of neutrophils, eosinophils, erythroid precursors, lymphoid cells, megakaryocytes (MKs), and morphologically immature myeloid precursors of 10 HPFs, and then by averaging the counts. The number of Ki-67$^+$ myeloid cells on BM sections from mouse chimeras was similarly assessed of 10 HPFs, and expressed as a mean.

Isolation, culture, and treatment of human and murine BM-MSCs

Human BM mesenchymal stromal cells (BM-MSCs) were obtained from aspirates of normal BM of patients undergoing hip replacement or Hodgkin lymphoma staging. The samples were obtained with informed consent per institutionally approved protocols, in accordance with the Declaration of Helsinki. The BM-MSC cultures were established from plastic-adherent BM cell fractions as detailed in supplemental Methods. Murine BM-MSCs were obtained from the trabecular fraction of femurs and tibias of WT and *Sparc*$^{-/-}$ mice as previously reported,[27] and cultures were established as detailed in supplemental Methods.

In vitro experiments on human and murine BM-MSCs were performed using cells between the second and fifth passages.

In vitro induction of human BM-MSCs toward osteoblastic or adipocytic differentiation was performed by the use of specific culturing media (StemCell Technologies) as detailed in supplemental Methods.

Stimulation with recombinant TGF-β1 (rTGF-β1) was performed on murine BM-MSCs obtained from WT and *Sparc*$^{-/-}$ mice. The cells were seeded into 6-well plates in complete medium at 70%-80% of confluence, starved for 24 hours in serum-free medium (Invitrogen), and treated with rTGF-β1 10 ng/mL (R&D Systems) for 48 hours before Western blot (WB) analysis.

For WB analysis, human and murine BM-MSC whole cell lysates were resolved by SDS-PAGE and transferred to nitrocellulose membranes (GE Healthcare).[25] The antibodies used are detailed in supplemental Methods. Densitometric analysis was performed using the ImageQuant TL Version 7 software (GE Healthcare Life Sciences).

Coculture experiments between WT or *Sparc*$^{-/-}$ murine BM-MSCs and WT lineage negative (Lin$^-$) hematopoietic cells have been performed according to Walenda et al,[28] as detailed in supplemental Methods.

Immunofluorescence and confocal microscopy

For in vitro immunofluorescence analysis, human and murine BM-MSCs were seeded into Fluorodish tissue culture dishes (World Precision Instruments), fixed in the plate with 2% PFA, and treated with 0.1% Triton X-100/PBS before incubation with the antibodies. The stained cells were analyzed under a RADiance-2000 (Bio-Rad) Nikon-TE300 laser scanning confocal microscope (Nikon).

For double-marker immunofluorescence on BM tissue, sections underwent 2 sequential rounds of single-marker immunostaining as previously reported.[9] The slides were evaluated under a Leica-TCS-SP5 laser scanning confocal microscope (Leica Microsystems) using HC PL APO 20×/0.70 and HCX PL APO CS 40×/1.25-0.75 objectives.

All of the antibodies used for immunofluorescence are detailed in supplemental Methods.

FACS analysis

FACS analysis was performed to assess the phenotype of human and mouse BM-MSCs, to determine the host or donor origin of the BM stromal cells in BM chimeras, and to evaluate the fractions of murine BM precursor populations (Lin$^-$c-kit$^+$, CMP, GMP, MEP) and circulating Gr1$^+$CD11b$^+$ myeloid cells. The antibodies used are detailed in supplemental Methods. Data were acquired using a BD Fortessa cytofluorimeter (BD Biosciences) and analyzed with FlowJo Version 8.8.6 analysis software (TreeStar).

BM colony formation assay

BM cells were obtained by flushing the femurs and tibias. The cells were then plated and cultured in MethoCult-GF-M3434 complete methylcellulose medium (StemCell Technologies), as previously described.[29] After 10 days, colonies were scored for colony-forming unit-granulocyte, -erythrocyte, -monocyte, -MK (CFU-GEMM), granulocyte-macrophage colony-forming unit (CFU-GM), and burst-forming unit-erythroid (BFU-E). Photomicrographs were collected following 2% PFA fixation under a Nikon-TM2000 microscope (Nikon) equipped with a Nikon-DXM1200 digital camera (Nikon).

GEP analysis

Whole transcriptome analysis was performed on data previously generated from different subsets of human BM mesenchymal and hematopoietic cells that was available at the NCBI Gene Expression Omnibus database (http://www.ncbi.nlm.nih.gov/geo/). For details, see supplemental Methods and supplemental Table 1.

GEP analysis was performed using GeneSpring Software (Agilent Technologies), as previously reported.[30] The EASE Version 2.0 software (National Institute of Allergy and Infectious Diseases, National Institutes of Health) was applied to establish whether specific cell functions and biologic processes, defined according to gene ontology, were significantly represented among the deregulated genes.[30]

Statistical analysis

Continuous and categorical variables were compared using the Mann-Whitney *U* test.

Correlation between variables was assessed using Pearson and Spearman coefficients. Analysis of the effects of TPO treatment and *Sparc* genotype on BM hematopoiesis was performed by 2-way ANOVA. Data were analyzed with the Statistical Package for the Social Sciences Version 13.0 (IBM) software.

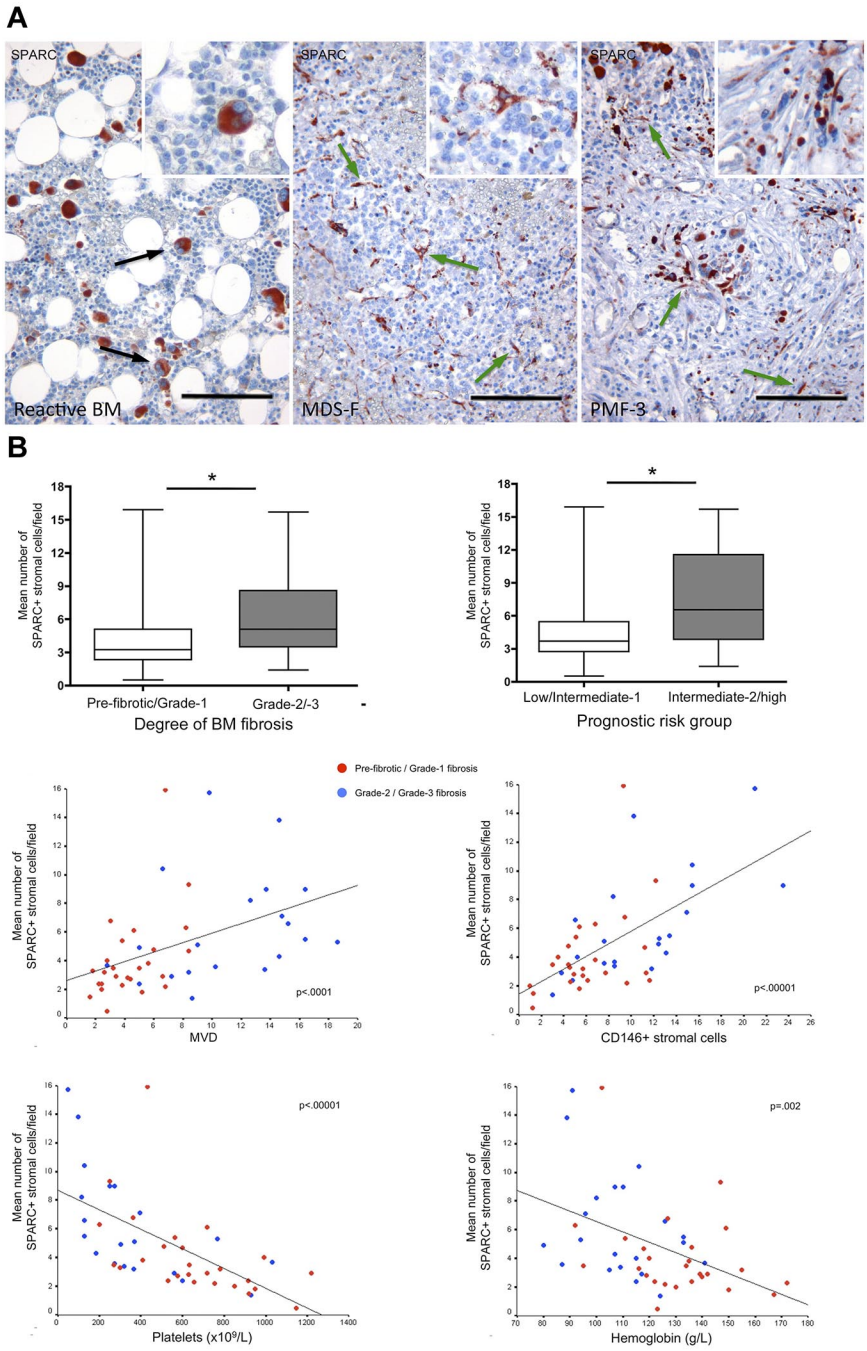

Figure 1. SPARC stromal expression and features of BM failure are correlated in myelofibrotic myeloid malignancies. (A) Immunohistochemical analysis of SPARC expression (aminoethyl-carbazole [AEC], red signal) on BM sections from control (Reactive BM) and myeloid neoplasm (MDS-F; PMF-3) cases. In normal BM that is free of stromal alterations, SPARC expression is confined to MKs (left panel, black arrows, inset). However, in marrow with myeloproliferation-associated stromal alterations, SPARC reactivity extends to stromal cells with spindle to stellate morphology (central and right panels, green arrows, insets). Three representative cases of the 114 cases evaluated are shown. Original magnifications ×200, insets ×630. Scale bars represent 100 μm. (B) The number of SPARC$^+$ stromal cells, assessed in 56 PMF cases, is significantly correlated with relevant biologic, clinical, and prognostic features: BM fibrosis; prognostic risk group according to Cervantes et al.[31] MVD; CD146$^+$ mesenchymal stromal cells. *$P < .05$. Box plot and scattergrams have been plotted to allow distinction between early (prefibrotic/grade 1 fibrosis) and advanced PMF cases (grade 2 or 3 fibrosis).

Results

SPARC stromal expression characterizes myeloid malignancies with BM stroma alterations and correlates with signs of BM failure

Because of the pleiotropic role of SPARC in tissue remodeling, we investigated whether its expression had any role in the stromal alterations associated with myeloid malignancies. Initially, we immunohistochemically tested SPARC expression in BMBs from 66 patients with different types of myeloid neoplasms and variable degrees of associated stromal changes, namely, BM fibrosis and/or osteosclerosis, and in 16 control BMBs. The clinical characteristics of these patients are summarized in Table 1.

In control cases and in myeloid neoplasms without associated stromal changes, such as essential thrombocytemia, early PV, and prefibrotic PMF, SPARC expression was confined to MKs (Figure 1A black arrows; supplemental Figure 2A). By contrast, in cases with significant stromal alterations, such as overt PMF, MDS with fibrosis (MDS-F), and acute panmyelosis with myelofibrosis, SPARC expression was also identified in spindle to stellate BM stromal cells intermingling with hematopoietic cells, branching around vessels or forming an intricate meshwork (Figure 1A green arrows; supplemental Figure 2A).

We subsequently investigated whether stromal SPARC expression correlated with histopathologic and laboratory variables of clinical significance in myelofibrotic myeloid neoplasms[5] using PMF as a prototypical model. The number of SPARC-expressing

stromal cells was assessed in 56 consecutive cases of PMF and correlated with the following variables: BM cellularity, degree of BM fibrosis, MVD, age, sex, Hb, complete PB counts, and PMF prognostic score according to Cervantes et al.[31] In addition, a correlation was made with the number of CD146-expressing BM-MSCs,[1,32] which we have reported to increase proportionally with the degree of stromal changes that occur along PMF progression (supplemental Figure 3).[9] The clinical and laboratory features of these PMF cases are summarized in Table 2.

We found that the number of SPARC$^+$ stromal cells correlated significantly with the degree of BM fibrosis (rho = 0.583, $P = .01$), MVD (rho = 0.550, $P < .0001$), and the number of CD146$^+$ BM-MSCs (rho = 0.632, $P < .00001$), reflecting the entity of stromal disarrangement (Table 2; Figure 1B). Moreover, the number of SPARC$^+$ stromal cells was higher in PMF patients belonging to a higher prognostic risk group (low/intermediate-1 vs intermediate-2/high, $P = .04$), and correlated with signs of BM hematopoietic failure, such as low Hb levels (rho = −0.429 vs Hb level, $P = .002$) and thrombocytopenia (rho = −0.539 vs PLT count, $P < .00001$; Table 2; Figure 1B). The significant difference in the mean number of SPARC$^+$ stromal cells per HPF among cases with different degrees of BM fibrosis was also confirmed in PV, MDS, and AML (supplemental Figure 2B).

These data indicate a correlation between SPARC stromal expression and the establishment of relevant BM fibrotic changes that parallel the progressive failure of normal BM hematopoiesis in PMF.

SPARC expression marks CD146$^+$ BM-MSCs and is associated with the osteoblastic milieu expansion underlying osteosclerotic progression

CD146$^+$ BM-MSCs are the mesenchymal precursors of BM stromal cells, including fibroblasts, BM reticular cells, adipocytes, and osteoblasts. In human BM, BM-MSCs display a spindle to stellate branching morphology and subendothelial distribution.[1,9,32] The concurrent changes in SPARC$^+$ cells and CD146-expressing BM-MSCs in PMF cases, and the morphology and distribution of several SPARC$^+$ stromal cells mirroring those of CD146$^+$ cells (Figure 2A black arrows), prompted us to test whether CD146$^+$ BM-MSCs were a source of SPARC in myeloid neoplasms with stromal alterations. Double immunofluorescence analysis for SPARC and CD146 in 30 cases of myeloid neoplasms with variable degrees of stromal fibrosis (range, 0-3, including 18 cases of PMF, 8 cases of PV, and 4 cases of MDS) showed that, aside from MKs and some stromal cells that were marked by SPARC but not CD146 (Figure 2B white arrows), SPARC expression overlapped that of CD146 in BM-MSCs displaying subendothelial localization (Figure 2B yellow arrows).

The BM stromal alterations associated with myelofibrotic myeloid malignancies may progress toward osteosclerosis (supplemental Figure 4), which could reflect an imbalance in the differentiative fate of BM-MSCs at the bifurcation between the osteoblastic and adipocytic differentiation, a checkpoint in which SPARC is involved (supplemental Figure 5).[33,34] We thus focused on the expression of SPARC and key ECM components of the osteoblastic niche, namely, collagen type I and fibronectin, in advanced PMF cases undergoing osteosclerotic progression. Expression of collagen type I and fibronectin, which was confined to the endosteal edge of the hematopoietic parenchyma in PMF cases without relevant stromal alterations (Figure 2C arrows), spread to the intertrabecular areas in cases with severe fibrosis and osteosclerosis (Figure 2C). Interestingly, in these cases, SPARC colocalized with collagen type I in sclerotic foci in situ (Figure 2D), as assessed by double immunofluorescence, and exhibited strong expression in osteoblasts at sites of osteosclerotic bone formation (Figure 2E arrows).

The in situ association between SPARC and foci of new bone formation was in line with the whole transcriptome GEP analysis that we performed on a panel of human samples representative of BM hematopoietic and mesenchymal cells (supplemental Table 1), including samples of BM-MSCs committed to osteoblastic differentiation. The list of *SPARC* best correlates (204 unique genes with Pearson correlation $r^2 > 0.95$; supplemental Table 2) was significantly enriched in key genes involved in cell adhesion/motility and communication (eg, *TGFB1* and *PDGFRA*), and ECM composition (supplemental Tables 2 and 3). Notably, among these, we found ECM genes involved as critical regulators of the osteoblastic milieu, such as *COL1A2, COL3A1, COL5A1/A2, COL12A1*, and *FN* (supplemental Figure 6).[35-37]

Altogether, these results associate SPARC with advanced osteosclerotic modifications, which may develop in myeloproliferative malignancies as a result of skewed BM-MSC differentiation dynamics.

Stromal SPARC is required for BM fibrotic changes accompanying TPO-induced reactive myeloproliferation

To investigate the relevance of SPARC in the induction of BM fibrotic changes associated with myeloproliferation, we adopted a murine experimental model of myelofibrosis. In mice, reactive myeloproliferation and associated stromal fibrosis could be induced by recombinant TPO treatment, as previously reported.[26] Thus, WT and *Sparc*$^{-/-}$ mice were treated intraperitoneally with TPO at a daily dose of 500 μg/kg for 10 or 14 days, killed, and analyzed for signs of myeloproliferation, and associated BM stroma alterations.

WT and *Sparc*$^{-/-}$ mice both developed myeloproliferation in the BM after 10 days of TPO treatment (Figure 3A). Myeloproliferation was paralleled by extramedullary splenic hematopoiesis with red pulp expansion (Figure 3B), PB thrombocytosis, and anemia (supplemental Figure 7A). BM histopathology and differential hematopoietic cell counts on BM sections highlighted that, differently from saline-treated controls, TPO-treated mice were characterized by increased BM cellularity with expansion of granulocytes and immature myeloid cells, and by MK hyperplasia with marked pleomorphism and cluster formation (Table 3; Figure 3A,C). Comparable results were obtained by 14 days TPO treatment (not shown).

In TPO-treated WT mice, myeloproliferation was associated with the development of moderate to severe stromal fibrosis and osteosclerotic foci (Figure 3A inset). Interestingly, none of the TPO-treated *Sparc*$^{-/-}$ mice displayed severe fibrosis or signs of osteosclerosis (Figure 3A). According to the histopathologic grading of BM fibrosis, which ranged from 0 to 3, the mean score of WT TPO-treated mice was 2.2 (SD, 0.76) compared with 0.8 of *Sparc*$^{-/-}$ mice (SD, 0.84; $P = .013$), whereas control marrows from both WT and *Sparc*$^{-/-}$ saline-treated mice scored 0 (Figure 3D). These in vivo results demonstrate that the absence of SPARC hampers the development of stromal fibrosis associated with TPO-induced reactive myeloproliferation.

To determine the cellular source of SPARC, either hematopoietic or stromal, relevant to the formation of BM stromal fibrosis, BM chimeras were generated in which WT or *Sparc*$^{-/-}$ mice were either donors or hosts, as well as Thy-1 (CD90) congenic. Because of the low Thy-1 expression in murine BM-MSCs, to verify whether BM stromal cells were substituted or not by BM transplantation,

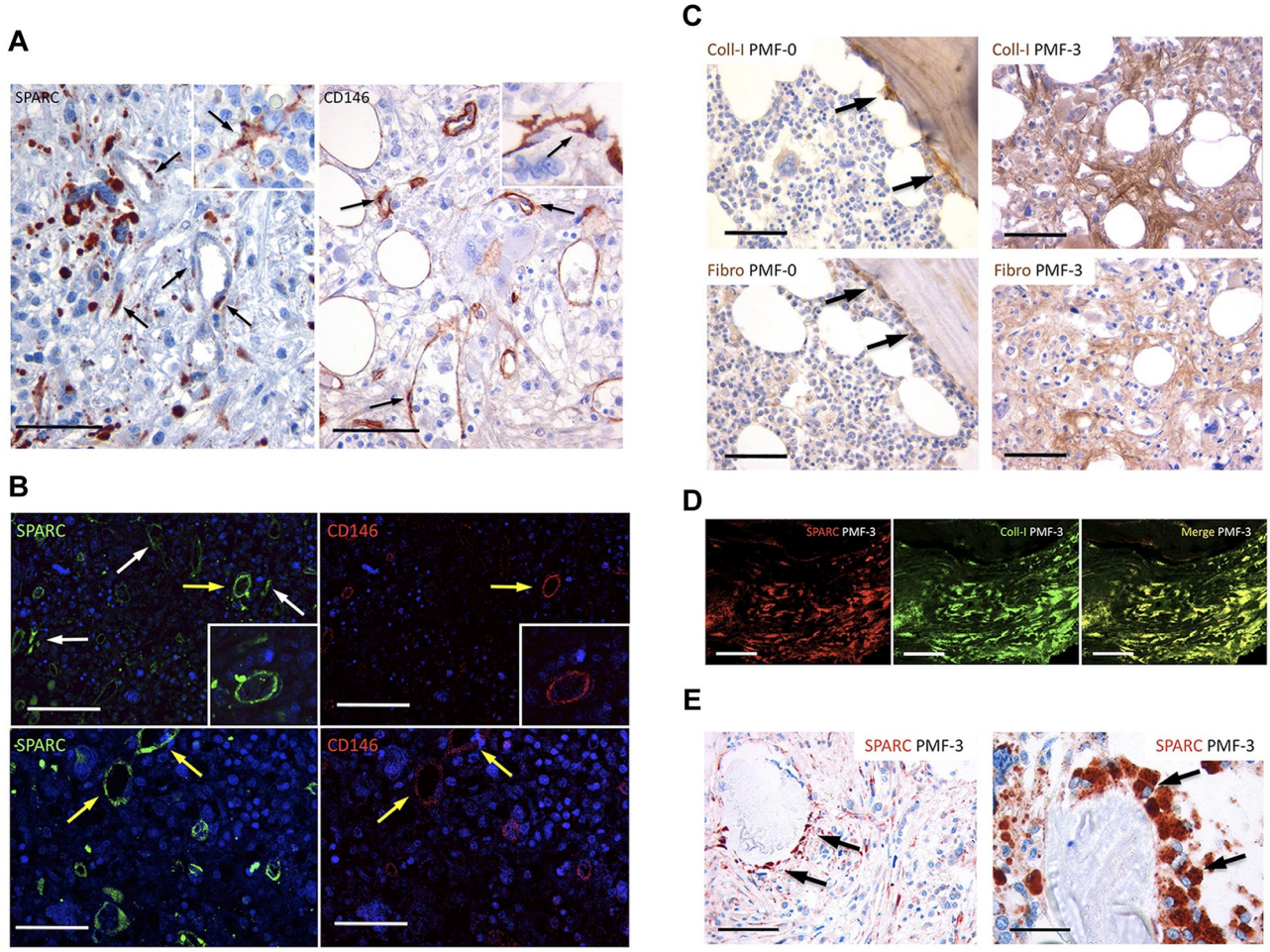

Figure 2. SPARC is expressed by CD146$^+$ BM-MSCs and associates with components of the expanded osteoblastic niche in osteosclerosis. (A) Immunohistochemical analysis of SPARC and CD146 (AEC, red signal) expression in PMF BM sections. Several SPARC-expressing stromal cells show subendothelial distribution and reticular morphology (black arrows, inset), which overlap those of CD146$^+$ BM-MSCs (black arrows, inset). Representative immunostained sections of the 114 evaluated are shown. Original magnifications ×400, insets ×630. Scale bars represent 50 μm. (B) Confocal microscopic analysis for SPARC (green signal) and CD146 (red signal) expression in PMF shows that, in addition to MKs and stromal cells expressing SPARC (white arrows), a subset of stromal cells with a perivascular distribution coexpresses SPARC and CD146 (yellow arrows and insets). Representative immunostained section of the 30 evaluated is shown. Original magnifications ×200 (top panels) and ×400 (bottom panels and insets). Scale bars represent 100 and 50 μm, respectively. (C) Immunohistochemical analysis for collagen type I (Coll-I) and fibronectin (Fibro; 3-3′-diaminobenzidine [DAB], brown signal) in sections from prefibrotic (PMF-0) and advanced PMF (PMF-3) cases. In the former (left panels), the 2 ECM components display selective localization at the endosteal edge of the bone trabeculae (black arrows) while undergoing a significant increase in expression and diffusion in the latter (right panels). Representative immunostained sections of the 30 evaluated are shown. Original magnifications ×400. Scale bars represent 50 μm. (D) Confocal microscopic analysis for SPARC (red signal) and collagen type I (Coll-I, green signal) expression showing that these 2 proteins colocalize in the sclerotic foci of an advanced PMF case (PMF-3). Representative immunostained sections of the 30 evaluated are shown. Original magnifications ×200. Scale bars represent 100 μm. (E) Immunohistochemical analysis of SPARC (red signal) showing its expression in osteoblasts (black arrows) lining bone trabeculae in myeloid malignancies undergoing osteosclerotic progression (PMF-3). Representative immunostained sections from 2 cases of the 30 evaluated are shown. Original magnifications ×400 (left panel) and ×630 (right panel). Scale bars represent 50 and 30 μm, respectively.

(CxB6)F1 mice expressing H-2K$^{b\text{-}d}$ MHC class I were transplanted with marrows from B6 mice expressing H-2K^b to follow MHC class I genotype in BM-MSCs. Flow cytometric analysis revealed that almost all of the nonhematopoietic CD44$^+$ and CD146$^+$ cells (gated on the CD45.2$^-$ population) expressed the host H-2K^d MHC class I molecule (supplemental Figure 8A), thus confirming that BM mesenchymal cells remained of host origin after transplantation.

Six weeks after BM transplantation, WT > WT, *Sparc*$^{-/-}$ > WT, WT > *Sparc*$^{-/-}$, and *Sparc*$^{-/-}$ > *Sparc*$^{-/-}$ chimeras were evaluated for reconstitution with donor hematopoietic cells and treated with high-dose TPO as detailed in "Methods." In all of the chimeras, TPO treatment induced significant myeloproliferation in the BM and spleen (Figure 4A-B; Table 4), thrombocytosis, and anemia (supplemental Figure 7B). The *Sparc* genotype of the radioresistant stroma was determinant for the development of myeloproliferation-related stromal changes. Indeed, although TPO-treated BM chimeras with host WT stroma showed marked fibrosis associated with myeloproliferation (Figure 4A, arrows), those with *Sparc*$^{-/-}$ recipient stroma developed slight or no fibrosis, regardless of the genotype of the BM donor. Specifically, the mean histopathologic scores of BM fibrosis for TPO-treated WT > WT and *Sparc*$^{-/-}$ > WT chimeras were 2.6 (SD, 0.55) and 2.8 (SD, 0.45), respectively, compared with 0.8 (SD, 0.55) of WT > *Sparc*$^{-/-}$ and 0.6 (SD, 0.89) of *Sparc*$^{-/-}$ > *Sparc*$^{-/-}$ chimeras (WT > WT vs WT > Sparc$^{-/-}$, $P = .004$; *Sparc*$^{-/-}$ > WT vs *Sparc*$^{-/-}$ > *Sparc*$^{-/-}$, $P = .001$; Figure 4C). The phenotype of such chimeras was consistent with the in situ SPARC expression detected by immunohistochemistry (supplemental Figure 8B).

These results confirm that SPARC contributes to the induction of BM stromal changes driven by myeloproliferation and identify BM stromal cells as the relevant source of SPARC in this setting.

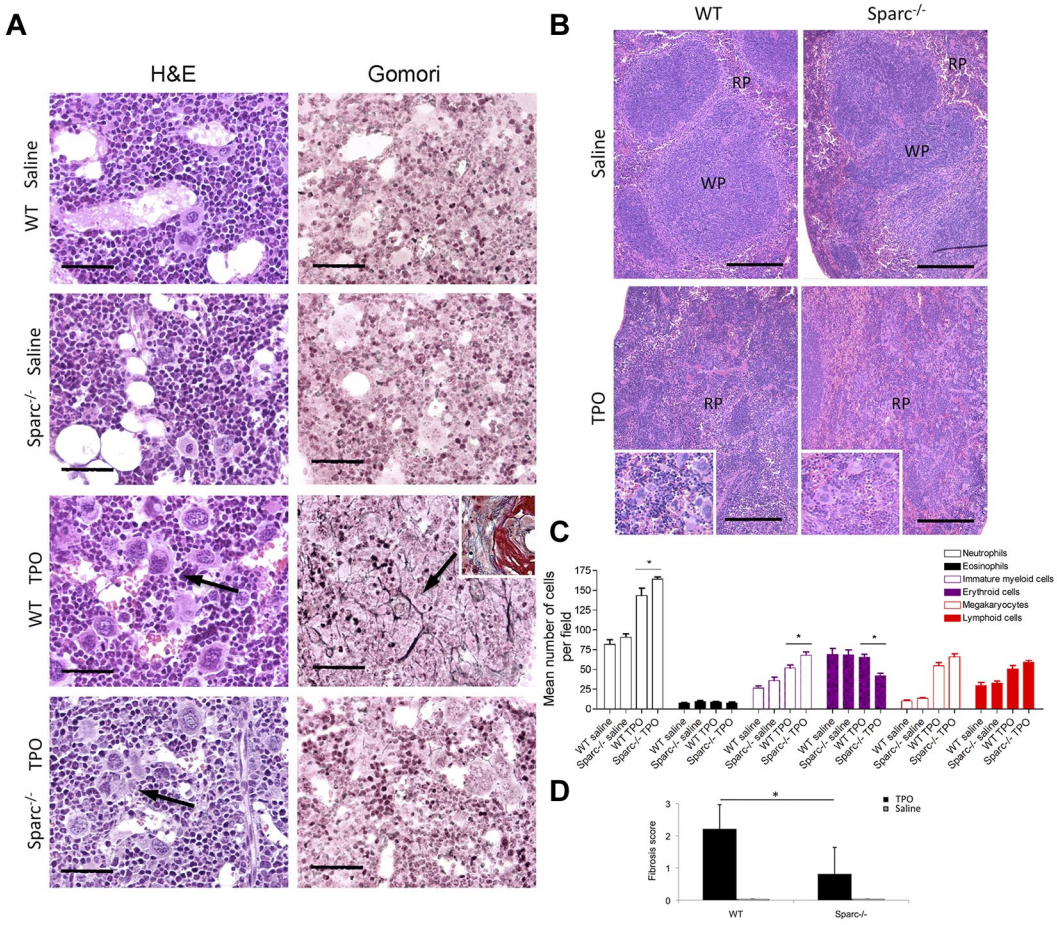

Figure 3. The development of TPO-induced experimental BM fibrosis in mice requires SPARC. WT and *Sparc*$^{-/-}$ mice were treated with recombinant TPO to induce myeloproliferation and fibrosis (n = 5 mice per condition, per experiment). Control mice were treated with the medium alone (sterile saline with 1% normal mouse serum). The data represent 1 experiment of the 3 performed. (A) Hematoxylin and eosin and Gomori staining of BM samples from TPO-treated WT and *Sparc*$^{-/-}$ mice. Hematoxylin and eosin staining shows that TPO administration induced granulocytic and megakaryocytic hyperplasia with MK atypia and cluster formation in both strains (hematoxylin and eosin panels, black arrows), which was not observed in sections from saline-treated mice. A significant degree of stromal fibrosis was observed in WT mice treated with TPO, which is highlighted by the presence of a network of black-stained fibers (Gomori panels, black arrow) and foci of osteosclerosis (Masson trichrome stain, inset). However, BM sections of TPO-treated *Sparc*$^{-/-}$ mice were completely free of signs of fibrosis similarly to the saline-treated WT and *Sparc*$^{-/-}$ mice (Gomori panels). Original magnifications ×400. Scale bars represent 50 μm. (B) Histopathologic analysis of the spleen architecture of control and TPO-treated WT and *Sparc*$^{-/-}$ mice showing that the splenic parenchyma of treated mice is characterized by effacement of the white pulp (WP) because of the expansion of the red pulp (RP) with prominent megakaryocytic hyperplasia and clustering (insets). Original magnifications ×100, insets ×200. Scale bars represent 200 μm. (C) Differential hematopoietic cell counts (mean ± SD) performed on BM sections of WT and *Sparc*$^{-/-}$ control and treated mice showing the significant increase in BM hematopoietic cells after TPO treatment. In each BM sample, the number of neutrophils, eosinophils, morphologically immature myeloid cells, erythroid cells, MKs, and lymphoid cells was counted of 10 HPFs. *$P < .05$. (D) Histopathologic grading of BM fibrosis in saline- and TPO-treated WT and *Sparc*$^{-/-}$ mice performed on Gomori-stained BM sections according to a 4-grade semiquantitative scoring system (see "Methods"). The mean grade of fibrosis is significantly higher in TPO-treated WT mice than in TPO-treated *Sparc*$^{-/-}$ mice. *$P < .05$.

Because chimeras with a *Sparc*$^{-/-}$ stroma failed to develop significant stromal alterations, we tested whether WT and *Sparc*$^{-/-}$ BM-MSCs respond differently to the prototypical epithelial-to-mesenchymal transition inducer TGF-β1 in vitro. BM-MSCs from WT and *Sparc*$^{-/-}$ mice, whose phenotype is reported in supplemental Figure 9, were starved for 24 hours in serum-free medium before the addition of rTGF-β1. After 48 hours, confocal microscopy analysis of SPARC expression and collagen type I deposition revealed that rTGF-β1 treatment induced up-regulation of SPARC and concurrent collagen type I fiber deposition in WT BM-MSCs (Figure 5A top panels), whereas *Sparc*$^{-/-}$ MSCs were refractory to TGF-β1-induced collagen deposition (Figure 5A bottom panels),

Table 3. Differential hematopoietic cell counts on BM sections in control and TPO-treated WT and Sparc$^{-/-}$ mice

	WT saline	Sparc$^{-/-}$ saline	WT TPO	Sparc$^{-/-}$ TPO	*P* value of treatment	*P* value of host SPARC genotype
Neutrophils	81 ± 12.3	92.8 ± 11.9	143.4 ± 19.9	163.8 ± 7.0	< .0001	.0208
Eosinophils	6.6 ± 2.1	13.4 ± 3.5	8.4 ± 2.9	7.6 ± 2.5	.9315	.3508
Immature myeloid cells	26.2 ± 6.3	35.8 ± 9.1	52 ± 7.6	68 ± 9.1	< .0001	.0208
Erythroid cells	69 ± 15.7	68.4 ± 13.6	65 ± 8.3	41.8 ± 6.9	.0101	.0375
Megakaryocytes	10.2 ± 2.8	13.4 ± 2.2	54.4 ± 8.9	65.8 ± 8.7	.0001	.0226
Lymphoid cells	29.8 ± 7.9	40.6 ± 12.2	50.8 ± 9.1	60.8 ± 7.1	.0001	.075

Data have been analyzed with a 2-way ANOVA. *P* value expresses how the treatment (TPO) and the *Sparc* host genotype affect the variables.

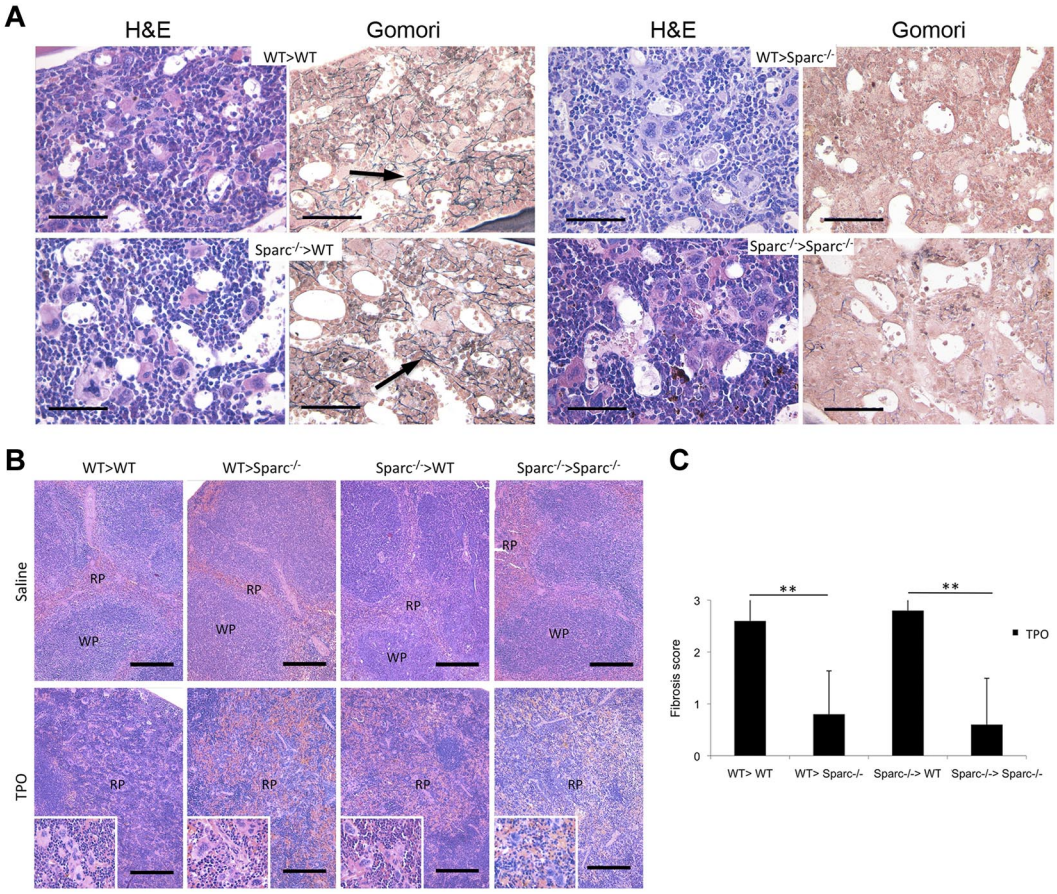

Figure 4. BM stromal cells are the relevant source of SPARC in the development of experimental BM fibrosis. BM chimeras were obtained by transplanting WT and *Sparc*$^{-/-}$ mice with either WT or *Sparc*$^{-/-}$ BM cells to obtain WT > WT, *Sparc*$^{-/-}$ > WT, WT > *Sparc*$^{-/-}$, and *Sparc*$^{-/-}$ > *Sparc*$^{-/-}$ BM chimeras. Chimeras were treated with either recombinant TPO to induce myeloproliferation and fibrosis or medium alone as a control (n = 5 mice per group, per experiment). The data shown represent 1 experiment of the 3 performed. (A) Histopathologic analysis of BM samples from TPO-treated BM chimeras. Hematoxylin and eosin staining shows signs of myeloproliferation in all of the different types of BM chimeras, which include marked granulocytic and megakaryocytic hyperplasia with MK clustering (hematoxylin and eosin panels). A considerable degree of dysgranulopoiesis and megakaryocytic atypia is observed in chimeras with a *Sparc*$^{-/-}$ recipient (WT > *Sparc*$^{-/-}$, *Sparc*$^{-/-}$ > *Sparc*$^{-/-}$). Gomori staining shows a significant degree of stromal fibrosis only in BM chimeras in which the recipient is WT (WT > WT, *Sparc*$^{-/-}$ > WT), as highlighted by the presence of an intricate network of black-stained fibers (Gomori panels, black arrows). By contrast, no stromal fibrosis is detected in TPO-treated chimeras in which the recipient is *Sparc*$^{-/-}$, irrespective of *Sparc* genotype of the donor. Original magnifications ×400. Scale bars represent 50 μm. (B) Histopathologic analysis of the splenic architecture of control and TPO-treated chimeric mice showing that the splenic parenchyma of treated mice is characterized by effacement of the white pulp (WP) because of the expansion of the red pulp (RP) with prominent megakaryocytic hyperplasia and clustering (insets). Original magnifications ×100, insets ×200. Scale bars represent 200 μm. (C) Grading of BM fibrosis in TPO-treated BM chimeric mice was performed on Gomori-stained BM sections according to a 4-grade semiquantitative scoring system (see "Histopathology and immunohistochemistry"). The mean grade of fibrosis is significantly higher in TPO-treated chimeric mice with a WT recipient than in those with *Sparc*$^{-/-}$ recipients. $^{**}P < .01$.

supporting that BM-MSCs intrinsically require SPARC for a proper fibrotic response. WB analysis confirmed the induction of SPARC up-regulation by TGF-β1 in WT BM-MSCs and showed that WT and *Sparc*$^{-/-}$ BM-MSCs differed in the cellular content of the mature collagen form (Figure 5B-C), which was only detectable in WT cells. Notably, TGF-β1, whose expression in WT cells paralleled SPARC modulation, was basally more expressed in *Sparc*$^{-/-}$ BM-MSCs and was slightly up-regulated after exogenous rTGF-β1 stimulation (Figure 5B), suggesting that defective collagen type I maturation and deposition occurring in the absence of SPARC were not the result of impaired TGF-β1 synthesis.

Therefore, the defective collagen matrix deposition characterizing *Sparc*$^{-/-}$ BM-MSCs is responsible for the reduced fibrosis of TPO-treated *Sparc*$^{-/-}$ recipient chimeras, as also supported by

Table 4. Differential hematopoietic cell counts on BM sections in control and TPO-treated chimeric mice

	WT > WT saline	WT > Sparc$^{-/-}$ saline	Sparc$^{-/-}$ > WT saline	Sparc$^{-/-}$ > Sparc$^{-/-}$ saline	WT > WT TPO	WT > Sparc$^{-/-}$ TPO	Sparc$^{-/-}$ > WT TPO	Sparc$^{-/-}$ > Sparc$^{-/-}$ TPO	*P* value of treatment	*P* value of host SPARC genotype
Neutrophils	89.6 ± 7.63	113.8 ± 13.0	114.0 ± 8.3	122.2 ± 5.4	138.7 ± 15.3	164.33 ± 19.3	156.2 ± 19.9	182 ± 8.13	< .0001	< .0001
Eosinophils	4.2 ± 1.8	3.0 ± 1.2	3.4 ± 1.1	4 ± 1.2	12.1 ± 3.2	10.5 ± 1.4	13.1 ± 2.9	12.3 ± 2.0	< .0001	.2443
Immature myeloid cells	31.6 ± 7.2	37.6 ± 9.8	41 ± 7.1	46.2 ± 4.1	46.3 ± 4.7	56.2 ± 5.5	44.3 ± 5.4	61.3 ± 6.6	< .0001	.0004
Erythroid cells	66.8 ± 10.3	69.2 ± 7.2	69.2 ± 5.11	68.8 ± 6.1	52.7 ± 9.5	40 ± 4.9	38.7 ± 7.5	33.5 ± 10.1	< .0001	.1241
Megakaryocytes	11.6 ± 3.6	11.6 ± 3.2	12.8 ± 2.4	14 ± 1.6	49 ± 2.3	62.3 ± 3.4	53 ± 13.0	74.8 ± 5.6	< .0001	< .0001
Lymphoid cells	44.6 ± 10.2	52.0 ± 13.8	54.6 ± 10.3	54.8 ± 8.7	46.8 ± 5.0	54.5 ± 4.9	34.5 ± 7.4	28 ± 7.6	.0011	.0405

Data have been analyzed with a 2-way ANOVA. *P* value expresses how the treatment (TPO) and the *Sparc* host genotype affect the variables.

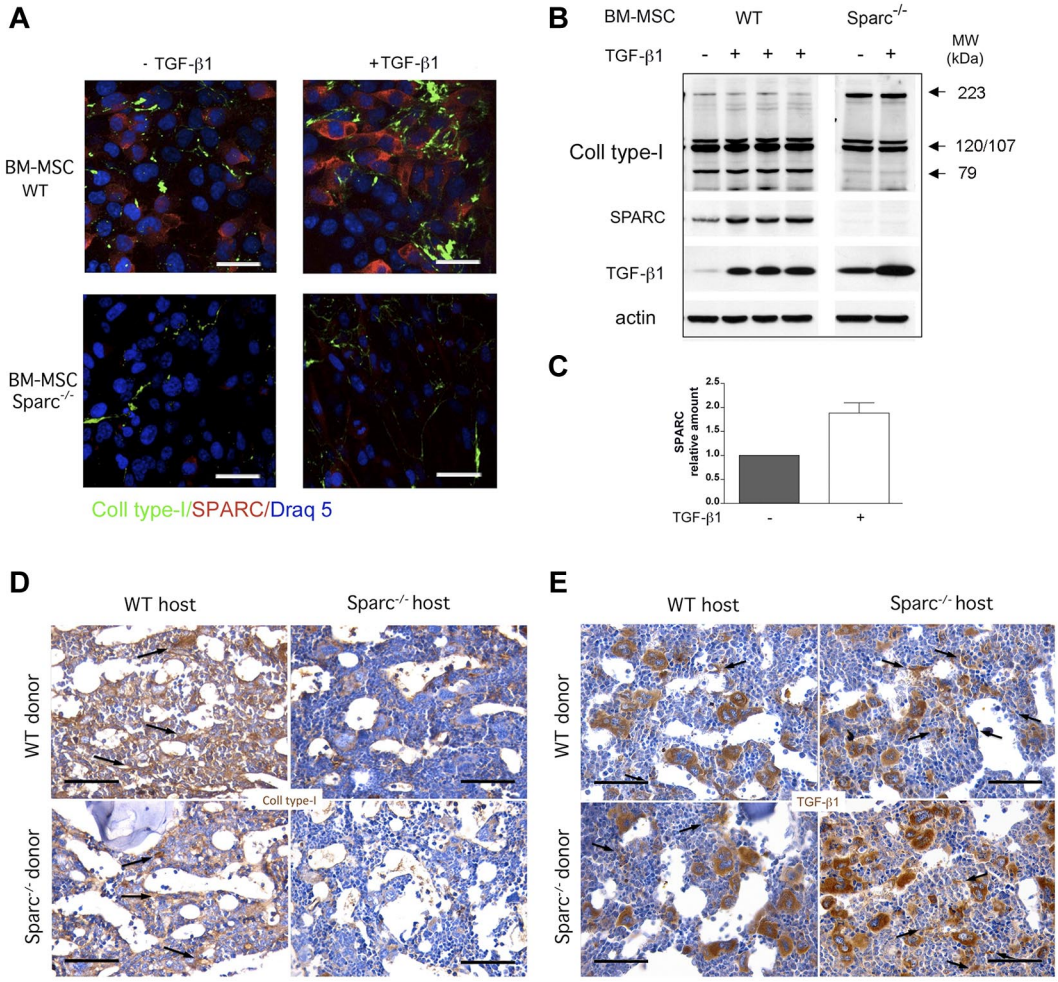

Figure 5. BM-MSCs from *Sparc*$^{-/-}$ mice are defective in collagen type I deposition despite high TGF-β1 synthesis. (A) In vitro confocal microscopic analysis for collagen type I (green) and SPARC (red) expression in BM-MSCs obtained from WT and *Sparc*$^{-/-}$ mice. BM-MSCs were seeded onto culture dishes adapted for confocal microscopy, starved for 24 hours, and then treated with recombinant TGF-β1. Untreated cells served as the control. The images show that rTGF-β1 administration induced SPARC up-regulation and collagen type I fiber deposition only in WT BM-MSCs. Results of 1 representative experiment of the 3 performed in triplicate are shown. Original magnifications ×400. Scale bars represent 50 μm. (B) Western blot analysis for collagen type I, SPARC, and TGF-β1 on whole cell lysates from BM-MSCs treated rTGF-β1. Untreated cells served as the control. Western blot analysis highlights a different pattern of collagen type I production by WT and *Sparc*$^{-/-}$ BM-MSCs. Specifically, WT BM-MSCs produce both the mature form of collagen (79 kDa) and precursors of low molecular weight (predicted molecular weight of 107-120 kDa). In contrast, *Sparc*$^{-/-}$ BM-MSCs were unable to produce the mature form of collagen (79 kDa) and accumulated precursors of high molecular weight (223 kDa), which indicates a defect in collagen maturation in *Sparc*$^{-/-}$, but not WT, BM-MSCs. WB analysis also showed that WT BM-MSCs up-regulate SPARC expression after rTGF-β1 administration. The results of 1 representative experiments of the 3 performed in triplicate are shown. (C) Western blot quantitative analysis of SPARC expression performed on WT BM-MSCs treated with rTGF-β1. Untreated cells served as the control. The data represent 1 experiment of the 3 performed in triplicate. (D) Immunohistochemical analysis of collagen type I expression (DAB, brown signal) in BM samples from mouse chimeras showing that chimeric mice with WT stroma (WT > WT, *Sparc*$^{-/-}$ > WT) have significantly higher interstitial deposition of collagen type I (left panels, black arrows) compared with chimeras with *Sparc*$^{-/-}$ BM stroma (WT > *Sparc*$^{-/-}$, *Sparc*$^{-/-}$ > *Sparc*$^{-/-}$; right panels). Four representative immunostained sections (1 per group) are shown of the 20 evaluated. Original magnifications ×400. Scale bars represent 50 μm. (E) Immunohistochemical analysis of TGF-β1 expression (DAB, brown signal) in BM samples from TPO-treated mouse chimeras showing that a higher density of BM stromal cells expressing TGF-β1 (arrows) is detected in chimeras with a *Sparc*$^{-/-}$ BM stroma (WT > *Sparc*$^{-/-}$, *Sparc*$^{-/-}$ > *Sparc*$^{-/-}$; right panels) compared with the WT counterpart (WT > WT, *Sparc*$^{-/-}$ > WT; left panels). Four representative immunostained sections (1 per group) are shown of the 20 evaluated. Original magnifications ×400. Scale bars represent 50 μm.

in situ defective expression of collagen type I in the presence of conspicuous TGF-β1 expression (Figure 5D-E). TGF-β1 was more expressed in the stroma of *Sparc*$^{-/-}$ recipient chimeras, than in WT counterparts (Figure 5E, arrows), which was consistent with the in vitro WB analysis of TGF-β1 expression on WT and *Sparc*$^{-/-}$ BM-MSCs.

SPARC deficiency in the BM stroma associates with an enhanced myelopoietic response to TPO

The analysis of BM chimeras, although crucial for dissecting the role of hematopoietic cell-derived and stroma-derived SPARC in BM fibrosis, uncovered that stroma-derived SPARC may affect myelopoiesis under a myeloproliferative stress, such as TPO treatment.

Indeed, TPO-induced reactive myeloproliferation in chimeras with a *Sparc*$^{-/-}$ stroma was characterized by increased granulopoiesis with enrichment of immature myeloid precursors, and by a higher degree of megakaryocytic hyperplasia with dysmegakaryopoiesis (ie, micromegakaryocytes with small hypolobulated nuclei) compared with chimeras with a WT stroma (Table 4; Figure 6A-B). Accordingly, a significant increase in myeloid colony forming units (CFU-GM; Figure 6C-D; WT > *Sparc*$^{-/-}$ vs WT > WT, $P = .038$; *Sparc*$^{-/-}$ > *Sparc*$^{-/-}$ vs *Sparc*$^{-/-}$ > WT, $P = .020$) and an increase in the fraction of GMP BM hematopoietic precursors

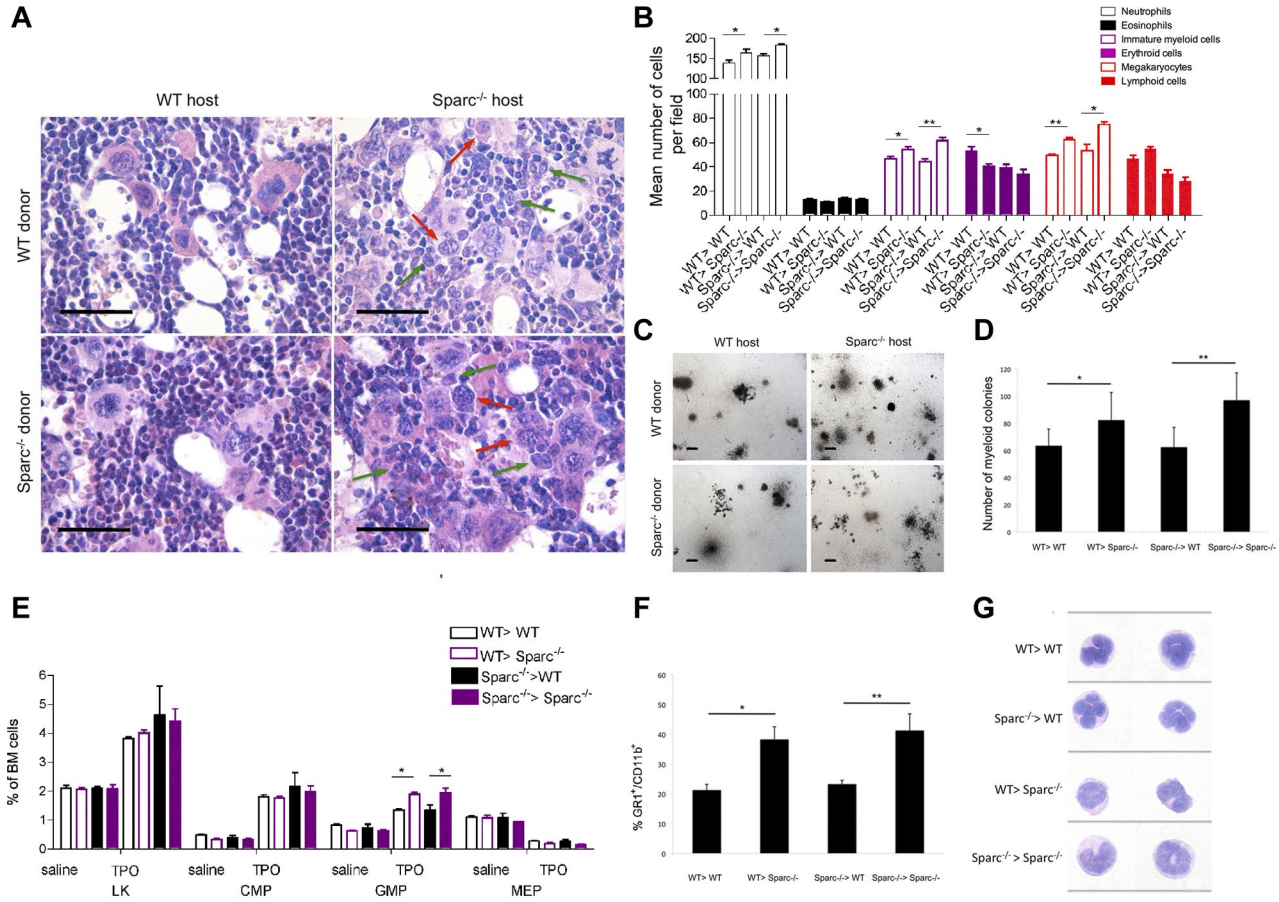

Figure 6. SPARC deficiency in the BM stroma associates with an enhanced myelopoietic response to TPO. (A) Histomorphologic analysis performed on hematoxylin and eosin-stained BM sections from TPO-treated mouse chimeras shows that mice with *Sparc*$^{-/-}$ stroma (WT > *Sparc*$^{-/-}$, *Sparc*$^{-/-}$ > *Sparc*$^{-/-}$) have significantly higher numbers of immature granulocyte precursors (green arrows) and highly atypical/dysplastic MKs (red arrows) compared with chimeras having WT stroma (WT > WT, *Sparc*$^{-/-}$ > WT). Four representative sections (1 per group) of the 20 evaluated are shown. Original magnifications ×400. Scale bars represent 50 μm. (B) Differential hematopoietic cell counts (mean ± SD) performed on BM sections of TPO-treated chimeric mice showing the different expansion of myeloid cell fractions of mice with a *Sparc*$^{-/-}$ or WT BM stroma. In each BM sample, the number of neutrophils, eosinophils, morphologically immature myeloid cells, erythroid cells, MKs, and lymphoid cells was counted of 10 HPFs. **P* < .05. ***P* < .01. Data are relative to counts performed on 2 different BM sections, per mice, per group. (C-D) Hematopoiesis in chimeric mice was analyzed using a clonogenic colony culture assay. BM cells from chimeric mice were seeded in Methocult M3434 for 10 days, and the colonies that formed were scored and photographed under an inverted microscope. (C) Representative images highlighting the enrichment of myeloid colonies in chimeric mice with *Sparc*$^{-/-}$ stroma. (D) The relative number of BM CFU-GM myeloid colonies (mean ± SD) is significantly increased in *Sparc*$^{-/-}$ recipient BM chimeras compared with WT recipient chimeras. **P* < .05. ***P* < .01. One representative experiment of the 3 performed with 5 mice per group is shown. (E) Hematopoietic progenitor cell numbers expressed as a percentage (mean ± SD) of total BM, showing the significant increase of GMP precursors in TPO-treated mice with *Sparc*$^{-/-}$ stroma compared with the WT counterparts. **P* < .05. The data represent 1 experiment of the 3 performed with 5 mice per group. (F) Flow cytometric analysis of Gr1^{+}CD11b^{+} circulating myeloid cells performed on the PB mononuclear cells of mouse chimeras. **P* < .05. ***P* < .01. The data represent 1 experiment of the 3 performed with 5 mice per group. (G) Morphologic analysis of hematoxylin and eosin-stained PB smears from BM chimeras show that circulating granulocytes from chimeric mice with *Sparc*$^{-/-}$ recipient stroma are enriched in immature forms, including pseudo-Pelger-Hüet and band-form nuclei, compared with circulating granulocytes from chimeras with WT stroma. Representative examples of circulating granulocytes from 2 smears per condition (of the 5 evaluated per experiment) are shown. Original magnifications ×1000.

(WT > *Sparc*$^{-/-}$ vs WT > WT, $P = .028$; *Sparc*$^{-/-}$ > *Sparc*$^{-/-}$ vs *Sparc*$^{-/-}$ > WT, $P = .029$; Figure 6E) were observed in TPO-treated chimeras with a *Sparc*$^{-/-}$ host genotype compared with the WT counterparts, suggesting that the expansion of selected myeloid progenitor cell populations was favored by SPARC stromal deficiency. Moreover, the number of Ki-67^{+} BM myeloid cells was significantly higher in WT > *Sparc*$^{-/-}$ (mean ± SD: 9.6 ± 1.50 cells/HPF) and *Sparc*$^{-/-}$ > *Sparc*$^{-/-}$ (10.1 ± 1.85 cells/HPF) chimeras compared with WT > WT (4.3 ± 1.16 cells/HPF) and *Sparc*$^{-/-}$ > WT counterparts (4.1 ± 0.99 cells/HPF; WT > *Sparc*$^{-/-}$ vs WT > WT $P < .001$; *Sparc*$^{-/-}$ > *Sparc*$^{-/-}$ vs *Sparc*$^{-/-}$ > WT $P = .001$; supplemental Figure 10A). Flow cytometric analysis on PB revealed a significant increase in the fraction of circulating Gr1^{+}CD11b^{+} myeloid cells in chimeras with *Sparc*$^{-/-}$ stroma compared with those with WT stroma (Figure 6F). In the PB smears of TPO-treated *Sparc*$^{-/-}$ recipients, a higher frequency of bandform stage immature granulocytes and pseudo-Pelger-Hüet figures (Figure 6G) were detected, further supporting the enhanced myelopoietic response to TPO in the absence of stromal SPARC.

The different support of *Sparc*$^{-/-}$ BM mesenchymal cells to myelopoiesis also emerged by in vitro coculture experiments in which Lin^{-} hematopoietic cells from WT mice were cocultured with either WT or *Sparc*$^{-/-}$ BM-MSCs in the presence of stem cell factor and TPO. After 7 days of coculture, hematopoietic cells were analyzed by FACS for expression of Gr1 and F4/80, which marked the fractions of Gr1^{+}F4/80^{-} granulocytes, Gr1^{-}F4/80^{+} monocytes, and Gr1 F4/80 double-positive or double-negative populations. In the presence of *Sparc*$^{-/-}$ BM-MSCs, a significantly higher fraction of Lin^{-} cells was driven toward granulopoiesis compared with that of Lin^{-} cells cocultured with WT BM-MSCs or cultured

alone (supplemental Figure 10B; $P = .0284$), indicating that the absence of SPARC in BM mesenchymal cells results in the favored expansion of specific myeloid cell populations.

Sparc deficiency in the BM microenvironment induces features of a myeloproliferative disorder in the presence of Apc^{min} mutant hematopoietic cells

The observation of an enhanced myelopoietic response to TPO in the presence of a *Sparc*$^{-/-}$ stroma prompted us to further investigate the influence of stromal *Sparc* deficiency over myeloproliferation. To this aim, BM cells from 8-week-old *Apc*^{min} mutant mice were transplantated into WT or *Sparc*$^{-/-}$ recipients. *Apc*^{min} BM cells were adopted because *Apc*^{min} mice display altered HSC function and defective quiescence and develop an MDS/MPD phenotype in the presence of HSC-extrinsic factors.[38,39]

Eight weeks after transplantation, chimeras were evaluated for reconstitution and myelopoiesis. *Apc*^{min} > *Sparc*$^{-/-}$ chimeras, but not *Apc*^{min} > WT chimeras, displayed features of a myeloproliferative disorder, which included BM myeloid hyperplasia with increased granulopoiesis and enrichment in morphologically immature myeloid cell clusters, as assessed by BM histopathology and immunohistochemistry for Gr1 (Figure 7A) and by differential BM hematopoietic cell count analysis (Figure 7B). FACS immunophenotypic characterization of BM precursors of *Apc*^{min} > *Sparc*$^{-/-}$ chimeras revealed a significant increase of the Lin$^-$ c-kit$^+$ precursors, and in particular of the GMP fraction compared with *Apc*^{min} > WT chimeras (Figure 7C-D; $P < .05$). The hypergranulopoiesis of *Apc*^{min} > *Sparc*$^{-/-}$ mice was also highlighted by PB FACS analysis, which revealed an expanded Gr1$^+$CD11b$^+$ circulating myeloid cell fraction (Figure 7E). The PB smears of *Apc*^{min} > *Sparc*$^{-/-}$ chimeras showed increase of circulating mature granulocytes and immature or blast-like myeloid cells (Figure 7F-G). Excess myelopoiesis in *Apc*^{min} > *Sparc*$^{-/-}$ chimeras was also detected in the spleen by histopathologic analysis, which revealed red pulp hyperplasia and partial effacement of the normal splenic architecture (Figure 7H), and by FACS analysis showing the increase of myeloid populations (supplemental Figure 11).

These results support the involvement of SPARC in the crosstalk between hematopoietic cells and the stromal microenvironment and suggest the contribution of SPARC stromal deficiency to the induction of local conditions favorable to myeloproliferation.

Discussion

Myeloproliferative conditions are paralleled by BM stroma remodeling events that variably involve modifications of the ECM, ranging from the slight changes of nonfibrotic disorders to the deep stromal disarrangement of osteosclerosis.[6] Stromal modifications may cast different influences on expanding myeloid populations and residual hematopoietic components. In this context, the functions of ECM proteins are poorly understood. In this study, we described a role for SPARC, a nonstructural protein of the ECM, as a stromal factor involved in the BM response to myeloproliferation. We investigated SPARC expression in myeloid malignancies with different degrees of associated stromal changes. SPARC was confined to hematopoietic cells in cases devoid of stromal fibrotic alterations, while being extensively expressed in stromal cells in myelofibrotic cases. In the prototypical setting of PMF, increased stromal SPARC expression correlated with the degree of stromal modifications, with a higher prognostic risk score, and with features reflective of impaired hematopoiesis, which implicated stromal SPARC in the detrimental scenario caused by BM fibrosis development and progression.

As a collagen chaperon involved in ECM assembly, SPARC has been investigated in fibrotic conditions, including pulmonary,[25] hepatic,[40] and renal fibrosis,[41] as well as cardiac infarction.[42] In these pathologic settings of inflammation-driven fibrosis, SPARC is expressed by stromal cells and hematopoietic immune cells, and its function is dependent on the cellular source. In bleomycin-induced lung fibrosis, SPARC produced by stromal and inflammatory cells promote collagen deposition and the resolution of inflammation, respectively.[25]

In myelofibrotic myeloid malignancies, stromal remodeling is not merely triggered by inflammation, although elevated pro-inflammatory cytokine levels have been described,[43] but rather it is sustained by the self-activity of the myeloid clone. Neoplastic myeloid cells synthesize a plethora of mediators, including TGF-β1, PDGFs, VEGFs, bFGF, and IGFs, which have been variably implicated in the pathogenesis of myelofibrotic changes.[6] It is conceivable that these factors, sensed by BM mesenchymal cells, could be responsible for the induction of SPARC stromal expression during myeloproliferation-related BM remodeling. Accordingly, the analysis of genes whose expression is significantly correlated with that of *SPARC* in BM hematopoietic and stromal cells highlighted the remarkable correlation between *SPARC* and some of the abovementioned axes (supplemental Table 2). These included *PDGFRA* and *TGFB1* ($r^2 = 0.96$ and $r^2 = 0.96$, respectively; supplemental Figure 12A), both implicated in the pathogenesis of myelofibrotic myeloproliferative neoplasms.[44,45] SPARC may directly interact with PDGFs to regulate their binding to cognate receptors.[46] In addition, a reciprocal regulation between SPARC and TGF-β1 in stromal cells emerges from in vitro and in vivo evidence,[42,47] including our results showing TGF-β1–induced up-regulation of SPARC in murine BM-MSCs. Therefore, SPARC expression in the BM stroma of myeloid neoplasms may be induced by clone-derived mediators, such as PDGFs and TGF-β1, in an attempt to restore homeostasis in the BM milieu. The persistence of myeloproliferation, which limits tissue normalization, would eventually divert the effects of SPARC expression toward detrimental fibrosis.

The role of SPARC in myelofibrosis development was investigated using a model of TPO-induced myelofibrosis in WT, *Sparc*$^{-/-}$ mice, in which SPARC proved to be required for the BM stromal remodeling triggered by reactive myeloproliferation. TPO experiments on BM chimeras, in which hematopoietic cells were of donor origin whereas stromal cells remained of host genotype, identified BM stromal cells as the relevant source of SPARC for the development of myeloproliferation-associated fibrosis. Moreover, in vitro stimulation of murine BM-MSCs with TGF-β1 showed defective collagen fiber deposition in *Sparc*$^{-/-}$ MSCs, which is a probable mechanism for the reduced fibrosis of TPO-treated chimeras retaining the host *Sparc*$^{-/-}$ stroma.

SPARC inhibition by RNA interference has been reported to effectively attenuate fibrosis in different cellular contexts, suggesting a possible application of this approach to fibrotic diseases.[40,48] A major caveat to the adoption of SPARC inhibition strategies in myeloproliferation-related BM fibrosis may come from our results showing that in the absence of stromal SPARC the myeloproliferative response to TPO was enhanced. Prompted by this observation, we investigated whether the selective SPARC deficiency in the BM stroma could favor myeloid cell expansion in the presence of a

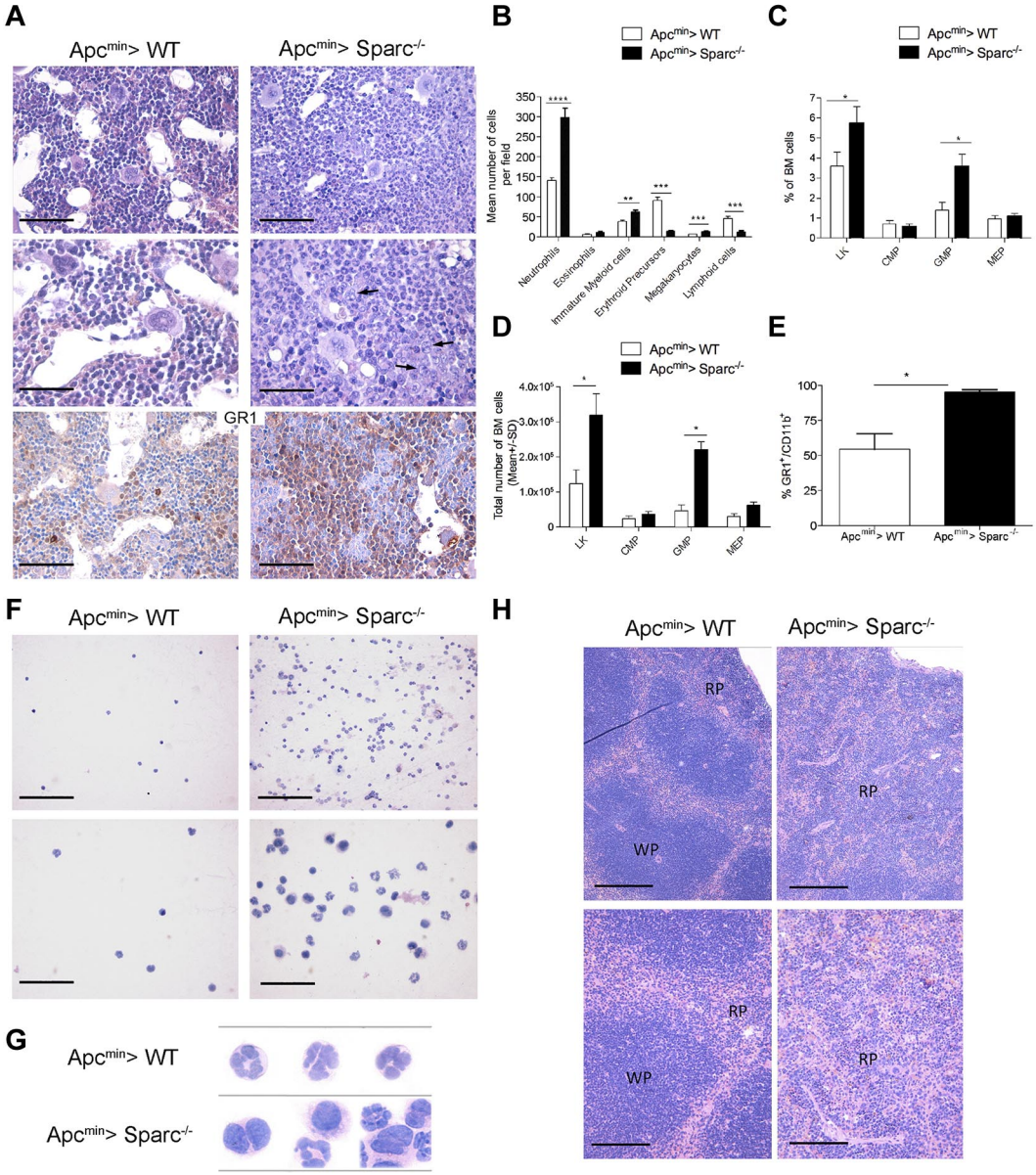

Figure 7. SPARC stromal deficiency induces features of a myeloproliferative disorder in the presence of *Apc*^{min} mutant hematopoietic cells. BM chimeras were obtained by transplanting BM hematopoietic cells from *Apc*^{min} donors into either WT or *Sparc*$^{-/-}$ recipients to obtain *Apc*^{min} > WT and *Apc*^{min} > *Sparc*$^{-/-}$ BM chimeras (n = 5 mice per group, per experiment). The data shown represent 1 experiment of 2 performed. (A) Histomorphologic and immunohistochemical analysis performed on BM sections from *Apc*^{min} > WT and *Apc*^{min} > *Sparc*$^{-/-}$ BM chimeras highlights that the BM of *Apc*^{min} > *Sparc*$^{-/-}$ (top right and middle right panels) chimeras is hypercellular compared with that of *Apc*^{min} > WT chimeras (top left and middle left panels) because of the marked expansion of mature granulocytes (marked by Gr1 in bottom panels, DAB, brown signal) and morphologically immature myeloid precursors. Four representative sections (1 hematoxylin and eosin-stained and 1 Gr1-immunostained, per group) of the 20 evaluated are shown. Original magnifications: top panels ×200, middle panels ×400, bottom panels ×200. Scale bars: top panels 100 μm, middle panels 50 μm, bottom panels 100 μm. (B) Differential hematopoietic cell counts (mean ± SD) performed on BM sections of *Apc*^{min} > WT and *Apc*^{min} > *Sparc*$^{-/-}$ BM chimeras show the prominent increase in the granulocyte myeloid cell fraction of *Apc*^{min} > *Sparc*$^{-/-}$ mice. In each BM sample, the number of neutrophils, eosinophils, morphologically immature myeloid cells, erythroid precursors, MKs, and lymphoid cells was counted of 10 HPFs. $^{**}P < .01$. $^{***}P < .001$. $^{****}P < .0001$. Data are relative to counts performed on 2 different BM sections, per mice, per group. (C-D) Fractions (C; percentage of total BM cells, mean ± SD) and absolute numbers (D; mean ± SD) of myeloid progenitor populations [Lin^{-}c-kit^{+} (LK), CMP, GMP, and MEP] showing the significant enrichment of GMP precursors in the BM of *Apc*^{min} > *Sparc*$^{-/-}$ chimeras compared with *Apc*^{min} > WT chimeras. $^{*}P < .05$. (E) Flow cytometric analysis of Gr1^{+}CD11b^{+} circulating myeloid cells performed on the PB mononuclear cells of *Apc*^{min} > WT and *Apc*^{min} > *Sparc*$^{-/-}$ chimeras showing the significant expansion of circulating granulocytes characterizing *Apc*^{min} > *Sparc*$^{-/-}$ mice. $^{*}P < .05$. (F) Hematoxylin and eosin-stained PB smears preparations of *Apc*^{min} > WT and *Apc*^{min} > *Sparc*$^{-/-}$ highlighting the granulocytosis associated with BM stroma SPARC deficiency. Representative areas from 2 smears (of 5 evaluated) per condition are shown. Original magnifications: top panels ×200, bottom panels ×400. Scale bars: top panels 100 μm, bottom panels 50 μm. (G) Morphologic analysis of hematoxylin and eosin-stained PB smears from BM chimeras show that circulating granulocytes from *Apc*^{min} > *Sparc*$^{-/-}$ are enriched in immature and blastlike forms compared with circulating granulocytes from chimeras with WT stroma. Representative examples of circulating granulocytes from 2 smears per condition (of the 5 evaluated per experiment) are shown. Original magnifications ×1000. (H) Histopathologic analysis of the spleen of *Apc*^{min} > WT and *Apc*^{min} > *Sparc*$^{-/-}$ chimeras showing that the splenic parenchyma of *Apc*^{min} > *Sparc*$^{-/-}$ mice is characterized by the expansion of the red pulp (RP) resulting from increased extramedullary myelopoiesis, and by the effacement of the white pulp (WP). Original magnifications: top panels ×100, bottom panels ×200. Scale bars: top panels 200 μm, bottom panels 100 μm.

genetically determined HSC defect linked with altered myelopoiesis, such as the one characterizing *Apc*^{min} mice.[38,39] In the *Apc*^{min} model, the enhanced HSC function and the defective quiescence resulting from increased Wnt-β-catenin signaling led to the development of an MDS/MPD phenotype, which requires the concurrence of HSC-intrinsic and microenvironmental factors.[38]

Therefore, the *Apc*^{min} represented a suitable experimental setting to investigate the influence of a SPARC-deficient microenvironment on MDS/MPD-prone HSC with preserved reliance on stromal signals. Transplantation of *Apc*^{min} BM cells into *Sparc*$^{-/-}$ recipients resulted in a myeloproliferative disorder classified in mice as "myeloproliferation-nonreactive,"[49] which was different from the MDS/MPD observed in *Apc*^{min} mice, underlining the driving contribution of the stromal environment to the outcome of the myeloproliferative spur. The myeloproliferative phenotype of *Apc*^{min} > *Sparc*$^{-/-}$ chimeras consisted of BM hypergranulopoiesis with increased numbers of circulating mature granulocytes and myeloid precursors and was not observed in *Apc*^{min} > WT chimeras, further indicating that SPARC deficiency in the BM stroma may represent a condition favoring myeloid expansion under a myeloproliferative stress. Recently, Siva et al have reported that SPARC is dispensable for murine hematopoiesis both at the steady state and under the stress induced by acute hemolysis or BM transplantation,[50] suggesting that SPARC deficiency does not alter the hematopoietic potential of the BM and that its contribution to the 5q− MDS phenotype may be subordinated to that of other molecular events that are not recapitulated in *Sparc*$^{-/-}$ models. We obtained similar results in the BM transplantion setting, in which *Sparc*$^{-/-}$ recipients were reconstituted without difference from WT recipients, even in the presence of low numbers of donor Lin$^-$ cells (ie, 2×10^3 cells, data not shown). This suggests that a true myeloproliferative spur complementing the total body irradiation is necessary to bring out the role of SPARC in myeloproliferation. Indeed, the enhanced myelopoietic response of mice with *Sparc*$^{-/-}$ BM stroma to TPO stimulation and to *Apc*^{min} hemopoietic cell transplantation indicates that the downstream effects of stromal SPARC synthesis, including collagen fibers assembly and deposition, may affect the control exerted by the BM stroma/HSC interaction over myelopoiesis.

The complex role of stromal SPARC in myeloproliferative conditions emerging from our experimental results is coherent with the homeostatic nature of matricellular proteins critically involved in tissue repair and normalization.[19] Some of these proteins, such as thrombospondin-1 and osteopontin, whose role in the pathogenesis of myelofibrotic myeloid neoplasms has been postulated, share with SPARC detrimental effects on the BM stroma homeostasis related to their up- or down-regulation in hematologic malignancies.[51-54]

Merging together our results from in situ expression analyses on human myeloid neoplasms and in vivo mouse models, we could hypothesize that the BM stroma response to myeloproliferative stimuli is entwined with the status of stromal SPARC expression. Increased or defective expression of SPARC in the BM stroma may exert different, yet detrimental, effects by fostering the development of fibrotic changes or inducing a flawed stromal niche permissive for the deregulated myeloid expansion, respectively. A possible limit to the generalization of this latter event related with defective stromal SPARC expression is represented by the evidence that in our models of TPO-induced reactive myeloproliferation and *Apc*^{min} > *Sparc*$^{-/-}$ transplantation the role of the stromal microenvironment was pivotal to the determination of the myeloproliferative phenotype. Indeed, this frame might not fit models of myeloproliferative disorders, such as those related with JAK2 or MPL gain-of-function mutations, in which hematopoietic cell-intrinsic defects are sufficient to determine the full-blown myeloproliferation in the absence of a recognized stromal contribution.[55] In this light, a role for BM stroma-derived SPARC may be envisaged in the early stress response of the BM microenvironment to myeloproliferation. Variations in SPARC stromal expression may allegedly be accomplices in the loss of BM hematopoietic homeostasis associated with stroma disarrangement and/or altered myelopoiesis.

Acknowledgments

The authors thank Dr Emilio Iannitto and Dr Umberto Gianelli for helpful discussion, Dr Ornella Pellerito and Dr Antonietta Notaro for precious assistance in the experimental procedures, and Mrs Mariella Parenza for technical help. The authors acknowledge the Confocal Microscopy Laboratory of the University of Palermo.

This work was supported by Associazione Italiana per la Ricerca sul Cancro (Program Innovative Tools for Cancer Risk Assessment and Diagnosis-5 per mille no. 12162 and Investigator Grant) and the Association for International Cancer Research.

Authorship

Contribution: C.T. and S.S. conceived the study and designed the research; C.G., P.P.P., G.C., M.C., G.F., C.C., M.S., S.M., M.G., A.C., A.M.F., and A.O. gathered data, performed the experiments, and analyzed the results; C.T., S.S., P.P.P., K.S., A.O., and M.P.C. wrote the manuscript; and S.A.P. and M.P.C. supervised the project and revised the manuscript.

Conflict-of-interest disclosure: The authors declare no competing financial interests.

Correspondence: Claudio Tripodo, Tumor Immunology Unit, Human Pathology Section, Department of Health Sciences, University of Palermo, Italy, Via del Vespro 129, 90127, Palermo, Italy; e-mail: claudio.tripodo@unipa.it; and Mario Paolo Colombo, Molecular Immunology Unit, Department of Experimental Oncology and Molecular Medicine, Fondazione Istituto di Ricovero e Cura a Carattere Scientifico Istituto Nazionale Tumori, Milan, Italy, Via Amadeo 42, 20133, Milan, Italy; e-mail: mario.colombo@istitutotumori.mi.it.

References

1. Bianco P. Bone and the hematopoietic niche: a tale of two stem cells. *Blood.* 2011;117(20):5281-5288.
2. Raaijmakers MH, Mukherjee S, Guo S, et al. Bone progenitor dysfunction induces myelodysplasia and secondary leukaemia. *Nature.* 2010; 464(7290):852-857.
3. Swerdlow SH, Campo E, Harris NL et al. *WHO Classification of Tumours of Haematopoietic and Lymphoid Tissues.* Lyon, France: IARC; 2008.
4. Corey SJ, Minden MD, Barber DL, Kantarjian H, Wang JC, Schimmer AD. Myelodysplastic syndromes: the complexity of stem-cell diseases. *Nat Rev Cancer.* 2007;7(2):118-129.
5. Vannucchi AM, Guglielmelli P, Tefferi A. Advances in understanding and management of myeloproliferative neoplasms. *CA Cancer J Clin.* 2009; 59(3):171-191.
6. Tripodo C, Sangaletti S, Piccaluga PP, et al. The bone marrow stroma in hematological neoplasms: a guilty bystander. *Nat Rev Clin Oncol.* 2011;8(8):456-466.
7. Thiele J, Kvasnicka HM, Facchetti F, Franco V, van der Walt J, Orazi A. European consensus on grading bone marrow fibrosis and assessment of cellularity. *Haematologica.* 2005;90(8):1128-1132.
8. Mesa RA, Hanson CA, Rajkumar SV, Schroeder G, Tefferi A. Evaluation and clinical correlations of bone marrow angiogenesis in myelofibrosis with myeloid metaplasia. *Blood.* 2000;96(10):3374-3380.
9. Tripodo C, Di Bernardo A, Ternullo MP, et al. CD146(+) bone marrow osteoprogenitors increase in the advanced stages of primary myelofibrosis. *Haematologica.* 2009;94(1):127-130.
10. Barbui T, Thiele J, Passamonti F, et al. Survival

and disease progression in essential thrombocythemia are significantly influenced by accurate morphologic diagnosis: an international study. *J Clin Oncol.* 2011;29(23):3179-3184.

11. Buesche G, Ganser A, Schlegelberger B, et al. Marrow fibrosis and its relevance during imatinib treatment of chronic myeloid leukemia. *Leukemia.* 2007;21(12):2420-2427.
12. Thiele J, Kvasnicka HM. Grade of bone marrow fibrosis is associated with relevant hematological findings: a clinicopathological study on 865 patients with chronic idiopathic myelofibrosis. *Ann Hematol.* 2006;85(4):226-232.
13. Vener C, Fracchiolla NS, Gianelli U, et al. Prognostic implications of the European consensus for grading of bone marrow fibrosis in chronic idiopathic myelofibrosis. *Blood.* 2008;111(4):1862-1865.
14. Della Porta MG, Malcovati L, Boveri E, et al. Clinical relevance of bone marrow fibrosis and CD34-positive cell clusters in primary myelodysplastic syndromes. *J Clin Oncol.* 2009;27(5):754-762.
15. Barbui T, Thiele J, Passamonti F, et al. Initial bone marrow reticulin fibrosis in polycythemia vera exerts an impact on clinical outcome. *Blood.* 2012; 19(10):2239-2241.
16. Tefferi A. Myelofibrosis with myeloid metaplasia. *N Engl J Med.* 2000;342(17):1255-1265.
17. Thiele J, Kvasnicka HM, Beelen DW, et al. Relevance and dynamics of myelofibrosis regarding hematopoietic reconstitution after allogeneic bone marrow transplantation in chronic myelogenous leukemia: a single center experience on 160 patients. *Bone Marrow Transplant.* 2000; 26(3):275-281.
18. Buesche G, Hehlmann R, Hecker H, et al. Marrow fibrosis, indicator of therapy failure in chronic myeloid leukemia: prospective long-term results from a randomized-controlled trial. *Leukemia.* 2003;17(12):2444-2453.
19. Chiodoni C, Colombo MP, Sangaletti S. Matricellular proteins: from homeostasis to inflammation, cancer, and metastasis. *Cancer Metastasis Rev.* 2010;29(2):295-307.
20. Piconese S, Costanza M, Tripodo C, et al. The matricellular protein SPARC supports follicular dendritic cell networking toward Th17 responses. *J Autoimmun.* 2011;37(4):300-310.
21. Clark CJ, Sage EH. A prototypic matricellular protein in the tumor microenvironment: where there's SPARC, there's fire. *J Cell Biochem.* 2008;104(3): 721-732.
22. Lehmann S, O'Kelly J, Raynaud S, Funk SE, Sage EH, Koeffler HP. Common deleted genes in the 5q− syndrome: thrombocytopenia and reduced erythroid colony formation in SPARC null mice. *Leukemia.* 2007;21(9):1931-1936.
23. DiMartino JF, Lacayo NJ, Varadi M, et al. Low or absent SPARC expression in acute myeloid leukemia with MLL rearrangements is associated with sensitivity to growth inhibition by exogenous SPARC protein. *Leukemia.* 2006;20(3):426-432.
24. Fenouille N, Puissant A, Dufies M, et al. Persistent activation of the Fyn/ERK kinase signaling axis mediates imatinib resistance in chronic myelogenous leukemia cells through upregulation of intracellular SPARC. *Cancer Res.* 2010;70(23): 9659-9670.
25. Sangaletti S, Tripodo C, Cappetti B, et al. SPARC oppositely regulates inflammation and fibrosis in bleomycin-induced lung damage. *Am J Pathol.* 2011;179(6):3000-3010.
26. Ulich TR, del Castillo J, Senaldi G, et al. Systemic hematologic effects of PEG-rHuMGDF-induced megakaryocyte hyperplasia in mice. *Blood.* 1996; 87(12):5006-5015.
27. Zhu H, Guo ZK, Jiang XX, et al. A protocol for isolation and culture of mesenchymal stem cells from mouse compact bone. *Nat Protoc.* 2010; 5(3):550-560.
28. Walenda T, Bokermann G, Ventura Ferreira MS, et al. Synergistic effects of growth factors and mesenchymal stromal cells for expansion of hematopoietic stem and progenitor cells. *Exp Hematol.* 2011;39(6):617-628.
29. Melani C, Sangaletti S, Barazzetta FM, Werb Z, Colombo MP. Amino-biphosphonate-mediated MMP-9 inhibition breaks the tumor-bone marrow axis responsible for myeloid-derived suppressor cell expansion and macrophage infiltration in tumor stroma. *Cancer Res.* 2007;67(23):11438-11446.
30. Piccaluga PP, De Falco G, Kustagi M, et al. Gene expression analysis uncovers similarity and differences among Burkitt lymphoma subtypes. *Blood.* 2011;117(13):3596-3608.
31. Cervantes F, Dupriez B, Pereira A, et al. New prognostic scoring system for primary myelofibrosis based on a study of the International Working Group for Myelofibrosis Research and Treatment. *Blood.* 2009;113(13):2895-2901.
32. Sacchetti B, Funari A, Michienzi S, et al. Self-renewing osteoprogenitors in bone marrow sinusoids can organize a hematopoietic microenvironment. *Cell.* 2007;131(2):324-336.
33. Delany AM, Kalajzic I, Bradshaw AD, Sage EH, Canalis E. Osteonectin-null mutation compromises osteoblast formation, maturation, and survival. *Endocrinology.* 2003;144(6):2588-2596.
34. Nie J, Sage EH. SPARC inhibits adipogenesis by its enhancement of beta-catenin signaling. *J Biol Chem.* 2009;284(2):1279-1290.
35. Pallotta I, Lovett M, Rice W, Kaplan DL, Balduini A. Bone marrow osteoblastic niche: a new model to study physiological regulation of megakaryopoiesis. *PLoS One.* 2009;4(12):e8359.
36. Kahai S, Vary CP, Gao Y, Seth A. Collagen, type V, alpha1 (COL5A1) is regulated by TGF-beta in osteoblasts. *Matrix Biol.* 2004;23(7):445-455.
37. Izu Y, Sun M, Zwolanek D, et al. Type XII collagen regulates osteoblast polarity and communication during bone formation. *J Cell Biol.* 2011;193(6): 1115-1130.
38. Lane SW, Sykes SM, Al-Shahrour F, et al. Apc(min) mouse has altered hematopoietic stem cell function and provides a model for MPD/MDS. *Blood.* 2010;115(17):3489-3497.
39. Wang J, Fernald AA, Anastasi J, Le Beau MM, Qian Z. Haploinsufficiency of Apc leads to ineffective hematopoiesis. *Blood.* 2010;115(17):3481-3488.
40. Atorrasagasti C, Aquino JB, Hofman L, et al. SPARC downregulation attenuates the profibrogenic response of hepatic stellate cells induced by TGF-beta1 and PDGF. *Am J Physiol Gastrointest Liver Physiol.* 2011;300(5):G739-G748.
41. Socha MJ, Manhiani M, Said N, Imig JD, Motamed K. Secreted protein acidic and rich in cysteine deficiency ameliorates renal inflammation and fibrosis in angiotensin hypertension. *Am J Pathol.* 2007;171(4):1104-1112.
42. Schellings MW, Vanhoutte D, Swinnen M, et al. Absence of SPARC results in increased cardiac rupture and dysfunction after acute myocardial infarction. *J Exp Med.* 2009;206(1):113-123.
43. Tefferi A, Vaidya R, Caramazza D, Finke C, Lasho T, Pardanani A. Circulating interleukin (IL)-8, IL-2R, IL-12, and IL-15 levels are independently prognostic in primary myelofibrosis: a comprehensive cytokine profiling study. *J Clin Oncol.* 2011;29(10):1356-1363.
44. Bock O, Loch G, Büsche G, von Wasielewski R, Schlué J, Kreipe H. Aberrant expression of platelet-derived growth factor (PDGF) and PDGF receptor-alpha is associated with advanced bone marrow fibrosis in idiopathic myelofibrosis. *Haematologica.* 2005;90(1):133-134.
45. Vannucchi AM, Bianchi L, Paoletti F, et al. A pathobiologic pathway linking thrombopoietin, GATA-1, and TGF-beta1 in the development of myelofibrosis. *Blood.* 2005;105(9):3493-3501.
46. Raines EW, Lane TF, Iruela-Arispe ML, Ross R, Sage EH. The extracellular glycoprotein SPARC interacts with platelet-derived growth factor (PDGF)-AB and -BB and inhibits the binding of PDGF to its receptors. *Proc Natl Acad Sci U S A.* 1992;89(4):1281-1285.
47. Francki A, Bradshaw AD, Bassuk JA, Howe CC, Couser WG, Sage EH. SPARC regulates the expression of collagen type I and transforming growth factor-beta1 in mesangial cells. *J Biol Chem.* 1999;274(45):32145-32152.
48. Wang JC, Lai S, Guo X, et al. Attenuation of fibrosis in vitro and in vivo with SPARC siRNA. *Arthritis Res Ther.* 2010;12(2):R60.
49. Kogan SC, Ward JM, Anver MR, et al. Hematopathology subcommittee of the Mouse Models of Human Cancers Consortium: Bethesda proposals for classification of nonlymphoid hematopoietic neoplasms in mice. *Blood.* 2002;100(1):238-245.
50. Siva K, Jaako P, Miharada K, et al. SPARC is dispensable for murine hematopoiesis, despite its suspected pathophysiological role in 5q− myelodysplastic syndrome [published online ahead of print April 5, 2012]. *Leukemia.* doi:10.1038/leu.2012.97.
51. Kopp HG, Hooper AT, Broekman MJ, et al. Thrombospondins deployed by thrombopoietic cells determine angiogenic switch and extent of revascularization. *J Clin Invest.* 2006;116(12): 3277-3291.
52. Evrard S, Bluteau O, Tulliez M, et al. Thrombospondin-1 is not the major activator of TGF-beta1 in thrombopoietin-induced myelofibrosis. *Blood.* 2011; 117(1):246-249.
53. Tefferi A. Pathogenesis of myelofibrosis with myeloid metaplasia. *J Clin Oncol.* 2005;23(33):8520-8530.
54. Liersch R, Gerss J, Schliemann C, et al. Osteopontin is a prognostic factor for survival of acute myeloid leukemia patients. *Blood.* 2012;119(22): 5215-5220.
55. Varricchio L, Mancini A, Migliaccio AR. Pathological interactions between hematopoietic stem cells and their niche revealed by mouse models of primary myelofibrosis. *Expert Rev Hematol.* 2009; 2(3):315-334.